Heliyon 10 (2024) e35085

Contents lists available at ScienceDirect

Heliyon

journal homepage: www.cell.com/heliyon

Research article

Energy efficiency research of propulsion system for series-parallel hybridization of amphibious vehicles

Xiaojun Sun [a,*], Fengmei Xin [b], Kun Gao [a]

[a] School of Automobile and Traffic Engineering, Liaoning University of Technology, Jinzhou 121000, China
[b] College of Science, Liaoning University of Technology, Jinzhou 121000, China

ARTICLE INFO

Keywords:
Amphibious vehicle
Gas-electric hybrid power
Energy flow
Series-parallel
Energy efficiency

ABSTRACT

The series-parallel hybrid system has attracted much attention from scholars for its effective integration of the power advantages and operating characteristics of different power sources, which is influenced by international emission regulations, energy-saving and emission reduction policies. As such, a series-parallel hybrid powertrain is introduced to the amphibious vehicle, and an innovative powertrain topology architecture is proposed. Meanwhile, the operation mode and energy efficiency characteristics are investigated during the working process. Firstly, the energy flow simulation model of a series-parallel gas-electric hybrid propulsion system is constructed using a modular modeling approach. Secondly, four operating modes, namely mechanical propulsion, electric propulsion, hybrid propulsion and charging mode, were formulated due to the fact that the propulsion system has multiple forms of power sources in the form of natural gas engine and reversible motor. Meanwhile, the energy flow states were investigated under different operating modes. Meanwhile, a comprehensive investigation of the energy efficiency associated with propulsion, storage and start-up energy was conducted for each specific mode. The results of the research indicated that the energy efficiency of the electric propulsion mode can reach up to 35.15 %, which is the gain from the wide operating range of the motor's high efficiency. The hybrid propulsion mode can obtain the highest energy efficiency of 35.88 %, which fully demonstrates the advantages of coordinating and complementing the two power sources, the natural gas engine and the reversible electric motor. This investigation also provides theoretical and empirical support for optimizing energy matching and formulating energy management strategies.

1. Introduction

Amphibious vehicles are special vehicles with the ability to travel on land and water, which have a unique design that allows them to demonstrate excellent maneuverability and adaptability in complex and changing terrain [1,2]. As the performance requirements of amphibious vehicles on the power system continue to improve, a simple powertrain type is difficult to meet the demand. Especially in high performance, flexibility and versatility, while effectively reducing energy consumption and pollutant emissions. All of the above are urgent issues facing current amphibious vehicle engineering [3,4]. For this reason, manufacturers and operators of amphibious vehicles are in urgent need of an innovative powertrain that addresses the pressing issues. Hybrid powertrains combine the

* Corresponding author.
E-mail address: 18245904309@163.com (X. Sun).

https://doi.org/10.1016/j.heliyon.2024.e35085
Received 3 March 2024; Received in revised form 17 July 2024; Accepted 22 July 2024
Available online 23 July 2024

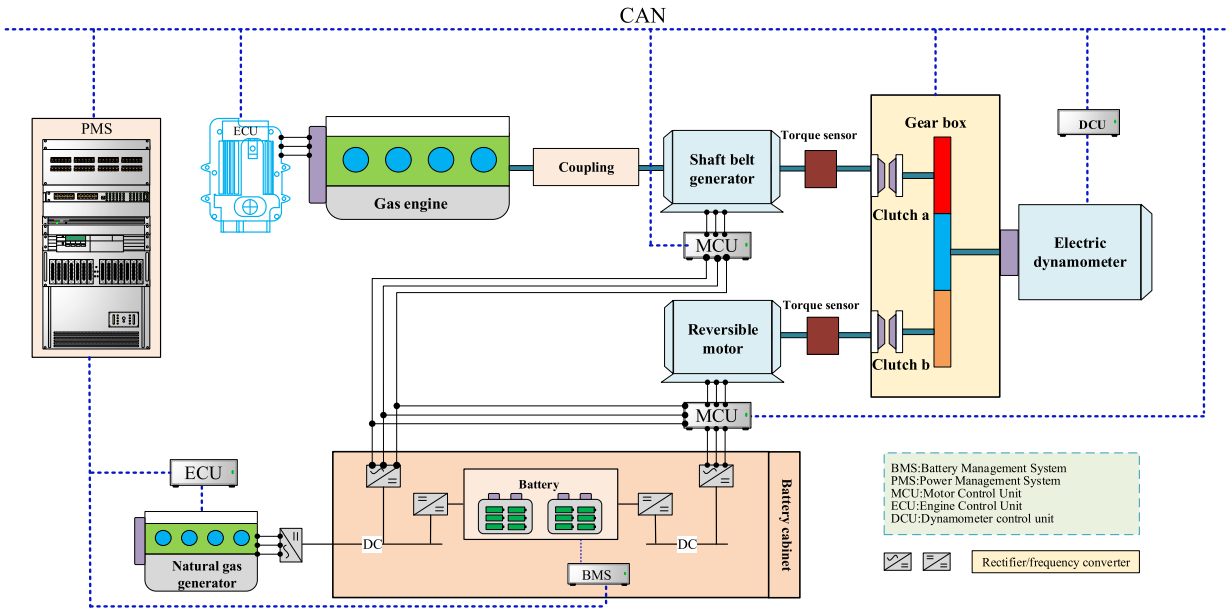

Fig. 1. Amphibious Vehicle Topology.(a)BMS:Battery Management System. (b)PMS:Power Management System; (c)MCU:Motor Control Unit; (d) ECU:Engine Control Unit; (e)DCU:Dynamometer Control Unit.

high-density energy output of conventional fuel power with the fast transient response of electric power to dramatically improve system efficiency and environmental performance [5,6]. Based on this, the focus of this article is not to start from the improvement of the power itself; rather, it is to find another way to propose a series-parallel power coupling type that can be used for amphibious vehicles to make up for the lack of power through power complementation.

Hybrid systems add an electrical drive system that makes power and economy tradeoffs possible. Hybrid systems have been applied to small cars [7], public transportation buses [8], marine vessels [9], and unmanned aerial vehicles [10]. Beatrice et al. [11] validated and analyzed energy management strategies for commercial plug-in hybrid electric vehicles using a testbed based on different operating conditions and driving styles. Dogdu et al. [12] compared the economic and emission performance of gasoline-powered vehicles with series hybrids using test conditions and a simulation platform. Zhou et al. [13] develop stochastic dynamic planning based fuzzy logic strategy to optimize the energy allocation of fuel cell hybrid buses. Liu et al. [14] presented a real-time nonlinear adaptive control strategy that can perform stability analysis for the problem of optimal energy allocation in fuel cell hybrid electric buses. Sun et al. [15] investigated the energy management of a natural gas engine-electric hybrid powertrain and proposed a novel predictive control strategy with a variable weight decision model. Li et al. [16] put forward a methanol-fueled marine hybrid power system consisting of a methanol engine, a solid-state battery, and a storage battery, and demonstrated the performance advantages of this power type from the perspective of carbon reduction. Xiao et al. [17] comprehensively synthesize the application scenarios and performance enhancement status of hybrid power systems in the field of unmanned aerial vehicles (UAVs). Yang et al. [18] proposal an energy allocation strategy based on a heuristic dynamic programming algorithm for large hybrid UAVs. It is evident from the above literature that hybrid power systems have been intensively researched for energy management and performance enhancement in small cars, public transportation buses, and marine vessels. In the field of amphibious vehicles, relevant topics are mainly researched from the perspectives of drag reduction technology [19], tail hydrofoil design [20], and energy saving and emission reduction technology [21]. However, the type layout of hybrid amphibious vehicles has not been explored in depth.

In the light of the above arguments, this document proposes a novel series-parallel gas-electric hybrid propulsion system applied to amphibious vehicles. Due to the coupling of multiple power sources, the hybrid powertrain can have multiple operational propulsion modes, thus maximizing energy efficiency based on mission requirements and fluctuating operating conditions. The in-depth analysis of the energy efficiency of different propulsion modes is known to be a crucial research work based on the above analysis and argumentation. The main contribution of this paper is to comprehensively explore the energy efficiency of the gas-electric hybrid propulsion system for series-parallel amphibious vehicles under different operating modes. The distribution of energy efficiency under different operating modes is revealed by energy flow paths and simulation models, which provides a theoretical basis for amphibious vehicle manufacturers, engineers and decision makers to make system layouts and matching selections.

The subsequent sections of this paper are structured into four main components. In Section 2, we elucidate the design of the series-parallel hybrid topology tailored for amphibious vehicles. Section 3 adopts a modular modeling approach to create a simulation model for the energy flow system. In Section 4, we carry out a comparative analysis of the operational modes and energy efficiency of the proposed solution. Lastly, we furnish the conclusions of this article.

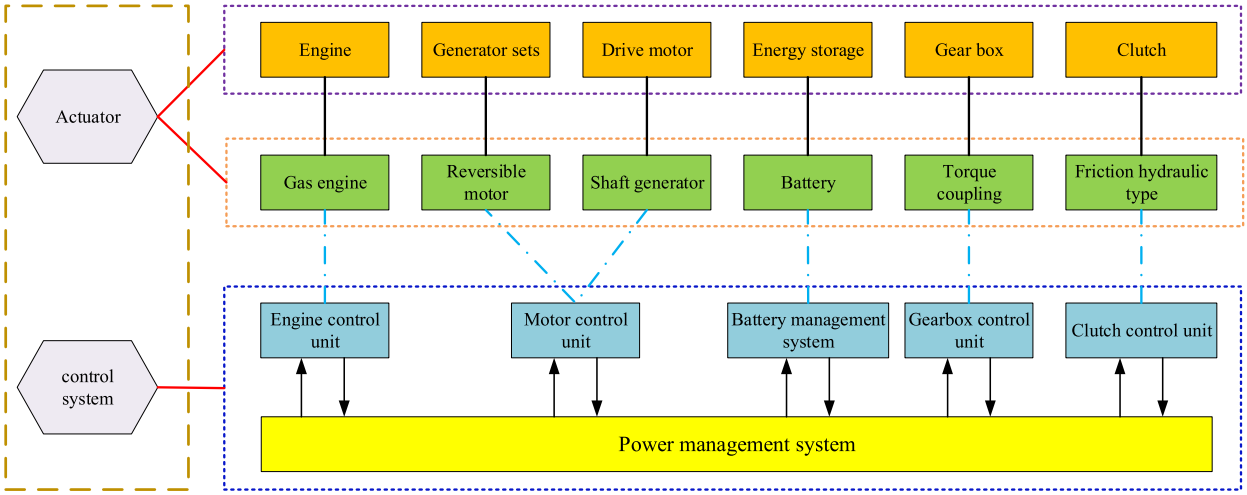

Fig. 2. Module composition unit.

Table 1
Equipment characteristics parameters.

No.	Equipment	Category	Parameters and Indicators
1	Gas engine	6M33	Cylinder type: six-cylinder , Turbocharger with Inter-cooling , four-stroke Displacement: 19.6 L Calibrated power: 330 kW Calibration speed: 1500 r/min Idling: 650 r/min
2	Reversible Motor/Shaft generator	Surface mount type	Rated power: 98 kW Rated voltage: 380 V Rated current: 285 A
3	Energy Storage	$LiFePO_4$	Battery energy: 205 kW h Continuous maximum output power: 102.8 kW Capacity: 315Ah Rated voltage: 652.8 V

2. The topology of series-parallel propulsion system

The topology of the series-parallel hybrid power system primarily comprises the following subsystems and components: a gas engine, a permanent magnet synchronous reversible motor, a generator with a shaft, an energy storage system, a clutch, a gearbox, and converter (including DC/DC converters, DC/AC inverters, AC/DC rectifiers, etc.). The power sources within the system encompass the gas engine, the permanent magnet synchronous reversible motor, the gas engine generator set, and the energy storage system. The control system encompasses the engine control unit, the motor control unit, the battery management system, the gearbox control unit, and the power management system. To fulfill the functional requirements of the system and implement the series-parallel mode effectively, we propose the comprehensive system configuration illustrated in Fig. 1. The modular composition of the hybrid power system is visually represented in Fig. 2.

The series-parallel hybrid power system for amphibious vehicles presented in this paper has the following advantages. Firstly, through the power conversion device, the system achieves efficient energy conversion and utilization, including energy recovery and reuse, which enhances energy utilization and extends the range. Moreover, the intelligent control system ensures precise control of the vehicle's power output, energy conversion, and storage, while maintaining system stability and safety under different operating conditions. In summary, the series-parallel hybrid system excels in optimizing energy utilization and intelligent control, making it capable of meeting the requirements of hybrid amphibious vehicles and providing them with reliable and efficient power support.

The main parameters of the equipment involved in the series-parallel propulsion system are illustrated in Table 1.

3. The construction of the propulsion system simulation model

Given the diverse components integrated into the hybrid propulsion system of amphibious vehicles, such as the gas engine, natural gas generator set, and batteries, the utilization of simulation analysis methods provides several distinct advantages. Firstly, it substantially diminishes research expenses by obviating the necessity for costly real-world experiments. Secondly, simulation analysis methods offer exceptional controllability, simplifying the simulation of intricate transient conditions and diverse extreme scenarios,

thereby accommodating a broad spectrum of research needs.

Considering the distinctive structure of the hybrid power system, this section will concentrate on the introduction of simulation models for three pivotal components: the engine, the reversible motor, and the energy storage system. The development and precision of these models hold paramount significance for evaluating and optimizing the hybrid power system's performance. A comprehensive simulation analysis can further deepen the understanding of the operating principles of the hybrid system, thus providing strong support for system improvement and performance enhancement.

3.1. The gas engine

The constructed gas engine model can accurately reflect the response characteristics in the dynamic working process. At present, the modeling methods for the engine are mainly bench experimental data simulation and theoretical derivation [22,23]. Theoretical derivation is chosen to be used for modeling in this paper for the sake of accurately reflecting the working state of the gas engine. The mass conservation equation, the energy conservation equation, and the ideal gas equation of state were employed to model the gas engine with a view to accurately capturing the trend of the gas engine during the dynamic process [24,25].

The gas engine model is primarily divided into the following subsystems: the gas fuel subsystem model, the cylinder and intake-exhaust subsystem model, the dynamic subsystem model, and the auxiliary subsystem model [26].

① The gas fuel subsystem model

The central role of the engine's gas fuel subsystem is to supply fuel to the cylinders. This fuel is drawn from the fuel storage tank, undergoes pressure stabilization via the gas fuel rail, and subsequently mixes with fresh air in the mixer. The key purpose of the gas fuel subsystem model is to simulate the dynamic variations in gas temperature and rail pressure within the gas fuel rail, thereby ensuring the adjustability of rail pressure and modeling the operation process of the mixer. Within this model, the most vital computed parameter is the mass flow rate of gas entering the cylinders, which is calculated as shown in Eq. (1).

$$mfio_k = \begin{cases} \sum \left(\frac{1}{1000} \frac{l_{gasvalve} \cdot A_{gasvalve} \cdot pio_k}{\sqrt{\left| \frac{Rio_k \cdot Tio_k}{2} \right|}} \right) & \text{if } \text{signal}_{injection} = 1 \\ 0 & \text{if } \text{signal}_{injection} = 0 \end{cases} \tag{1}$$

where $mfio_k$ represents the mass flow rate of methane at the inlet of the gas rail (kg/h); $l_{gasvalve}$ is the lift of the gas valve (m); $A_{gasvalve}$ is the flow area of the gas valve (m^2); pio_k is the methane pressure at the inlet of the gas rail (Pa); Rio_k is the methane gas constant at the inlet of the gas rail; Tio_k is the temperature of methane gas at the inlet of the gas rail (K); $\text{signal}_{injection}$ is the jet control signal.

② The cylinder and intake-exhaust subsystem model

The cylinder and intake-exhaust subsystem models hold a central role within the gas engine model. The cylinder subsystem replicates the working conditions within the cylinder, computing changes in cylinder pressure and the rate of combustion heat release, along with the influence of fuel injection and rail pressure on combustion characteristics. In contrast, the intake-exhaust subsystem emulates variations in the state of compressed air, the control process of intake and exhaust valves, and the intercooling process during air compression. The parameters computed from these subsystem models significantly contribute to comprehending the performance of the gas engine, encompassing vital parameters such as indicated torque and heat dissipation rate. The formula for calculating the combustion heat release rate in the cylinder is depicted in Eq. (2).

$$\frac{dQ_b}{d\phi} = \begin{cases} H_{uo} \cdot misCH4_k \cdot \frac{dx}{d\phi} & \alpha aiskcyc \geq 1 \\ \frac{H_{uo} \cdot (mis_k \cdot misCH4_k)}{17.2 \frac{dx}{d\phi}} & \alpha aiskcyc < 1 \end{cases} \tag{2}$$

where $\frac{dQ_b}{d\phi}$ is the instantaneous heat release rate of each cylinder's fuel (J/deg); H_{uo} is the low-temperature calorific value of natural gas (J/kg); mis_k is the internal gas mass of each cylinder (kg); $\frac{dx}{d\phi}$ is the combustion rate of each cylinder (1/deg); $misCH4_k$ is the mass of natural gas inside each cylinder (kg); $\alpha aiskcyc$ is the excess air coefficient per cycle inside each cylinder.

The formula for calculating indicated torque is shown in Eqs. (3)–(8).

$$T_i = \frac{\sin(\theta + \beta)}{\cos \beta} \cdot \left(P_g + P_j\right) \cdot R \tag{3}$$

$$\theta = \begin{cases} \dfrac{\pi \cdot \theta}{180} & \phi \in (0, 180) \\ \dfrac{-\pi(\phi - 180)}{180} & \phi \in (180, 360) \\ \dfrac{\pi(\phi - 360)}{180} & \phi \in (360, 540) \\ \dfrac{-\pi(\phi - 540)}{180} & \phi \in (540, 720) \end{cases} \tag{4}$$

$$\sin\beta = \gamma \sin\theta \tag{5}$$

$$P_g = \frac{\pi D^2}{4}(Pis_k - P_s) \tag{6}$$

$$P_j = -m\mathrm{Rec}ip \cdot a \tag{7}$$

$$a = R\omega^2\left(\cos\alpha + \gamma\frac{\cos 2\theta}{\cos\beta} + \frac{\gamma^3}{4}\cdot\frac{\sin^2 2\theta}{\cos^2\beta}\right)\alpha = R\omega^2\left(\cos^{-1}\theta\right) \tag{8}$$

where T_i represents the indicated torque of each cylinder (N·m); θ calculates the crankshaft angle (rad) for the indicated torque of each cylinder; β is the angle (rad) between the connecting rod of each cylinder and the centerline of the cylinder; P_g is the force at the top of each cylinder piston (N); P_j is the reciprocating inertia force between the small end of each cylinder connecting rod and the piston (N); R is the crank radius of each cylinder (m); ϕ is the crankshaft angle (deg); γ is the crank to connecting rod ratio; D is the piston diameter (m); Pis_k is the internal gas pressure of each cylinder (Pa); P_s is the environmental pressure (crankcase pressure) (Pa); $m\mathrm{Rec}ip$ is the sum of the small end masses of the piston and connecting rod (kg); a is the acceleration of the piston movement in each cylinder (m/s^2); n_{eng} is the engine speed (r/min).

③ The dynamic subsystem model

The core function of the engine's dynamic subsystem model, grounded in dynamic equations, is to compute the actual engine speed. It accomplishes this by simulating the impact of friction torque and load torque on the engine speed and accounting for the influence of cooling water temperature on friction torque. The principal calculated parameters within this subsystem encompass the actual engine speed, starting torque, friction torque, effective torque, and various others. These parameters hold significant importance in the examination and enhancement of the engine's dynamic performance.

The formula for calculating the effective torque of the gas engine is shown in Eq. (9).

$$T_{eng} = T_i - T_f \tag{9}$$

where T_e is the effective output torque (N·m); T_i is the indicated torque (N·m); T_f is the frictional torque (N·m).

The formulas for calculating the engine speed are shown in Eqs.(10) and (11).

$$\frac{dn_{eng}}{dt} = \frac{60}{2\pi}\cdot\frac{T_i + T_s - T_f - T_{l\_e}}{J_e} \tag{10}$$

$$n_{eng} = n_0 + \int\frac{dn_{eng}}{dt}\cdot dt \tag{11}$$

Where n_0 is the initial engine speed (r/min); T_s is the starting torque (N·m); T_{l_e} is the engine load torque (N·m).

④ The auxiliary subsystem model

The auxiliary subsystem model serves to calculate parameters related to the cooling system and lubrication system. This includes variables like internal circulation freshwater temperature, lubricating oil temperature, and lubricating oil pressure. For instance, the formula for calculating the internal circulation cooling water temperature is detailed in Eqs.(12)–(14).

$$T_k = T0_k + \int(dT_k \cdot dt)dt \tag{12}$$

$$dT_k = \frac{\left(\sum\frac{dQ_w}{dt}\right) - \frac{dQ}{dt}he}{4200 \cdot m_k} \tag{13}$$

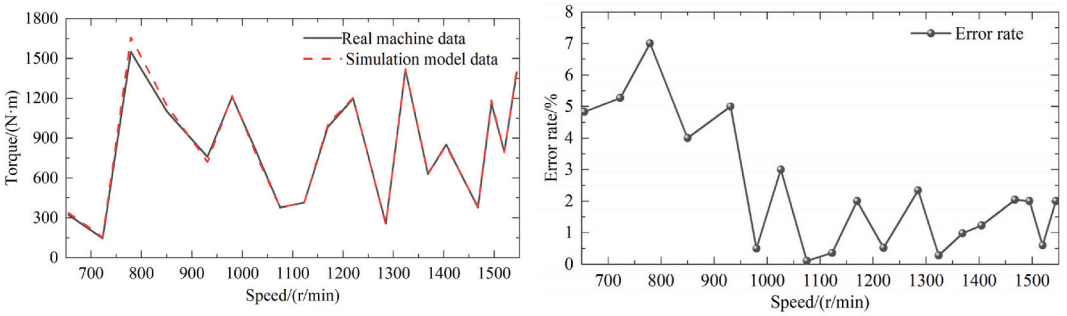

(a) Torque output comparison (b) Error rate

Fig. 3. Comparison of real machine and simulation.

$$\frac{dQ}{dt}_{he} = \eta_{he} \cdot \alpha_{he} \cdot A_{he} \cdot (T_k - T0_{sea}) \tag{14}$$

where T_k is the temperature of internal circulating fresh water (K); $T0_k$ is the initial temperature of the internal circulating fresh water (K); dT_k is the temperature and flow rate of internal circulating fresh water (K/s); $\frac{dQ_w}{dt}$ is the rate of change in heat transfer around the walls of each cylinder (J/s); $\frac{dQ}{dt_{he}}$ is the heat exchange capacity of the heat exchanger (J/s); m_k is the total mass of internal circulating fresh water (kg); η_{he} is the heat exchange efficiency of the sea fresh water heat exchanger; T_k is the temperature of the internal circulating fresh water (K); α_{he} is the thermal conductivity of the sea fresh water heat exchanger; A_{he} is the heat exchange area of the sea fresh water heat exchanger (m^2); $T0_{sea}$ is the temperature of the external circulating seawater (K).

The above mathematical modeling shows that the efficiency of the gas engine is calculated as indicated in Eq. (15).

$$\eta_{eng} = \frac{\frac{\pi}{30} n_{eng} T_{eng}}{\frac{H_{uo} \int_{t_k}^{t_{k+1}} mfio_k dt}{3.6(t_{k+1} - t_k)}} \times 100 \tag{15}$$

The offline, semi-physical simulation experiments are meaningful only when the accuracy of the controlled object model reaches certain requirements. Some operating points of the gas engine were selected to calibrate the engine against the simulation model to verify the model accuracy. The main function of the constructed gas engine model is to simulate the input and output characteristics of the actual gas engine as a whole, hence the output torque of the gas engine model is chosen to be compared with the actual values as presented in Fig. 3. The comparison of the simulated output torque of the gas engine with the experimental data reveals that the simulated output basically coincides with the experimental data, as reflected in Fig. 3(a). The maximum error rate did not exceed 10 %, as illustrated in Fig. 3(b). As a whole, the established simulation model can reflect the actual working process of the gas engine with high accuracy and can be applied to the next energy flow analysis.

The space-filling experimental design method was used to design the experimental points of the gas engine, using the constructed model the gas flow was simulated and the gas flow distribution was obtained as illustrated in Fig. 4. The efficiency of the gas engine at a certain operating condition is calculated using Eq. (15) to provide a reference efficiency for the next energy flow calculations.

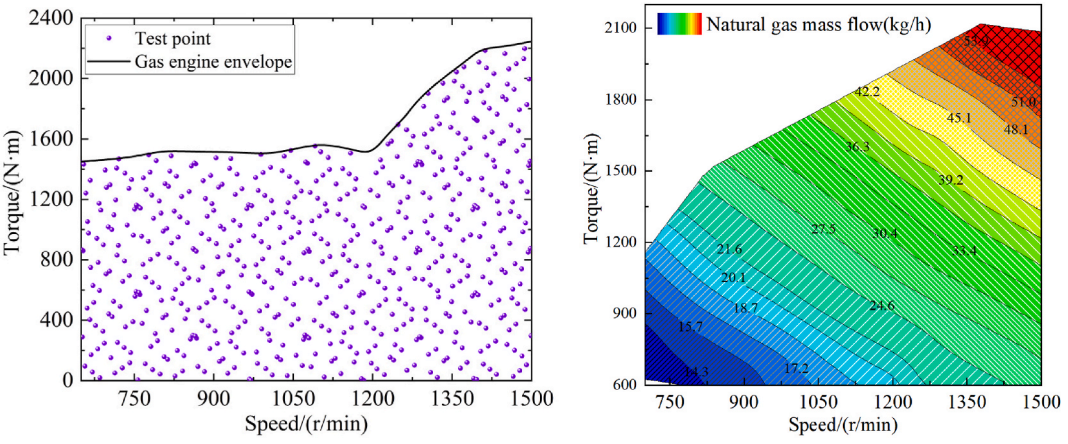

(a) Test point (b) Natural gas mass flow simulation results

Fig. 4. Test design and presentation of results.

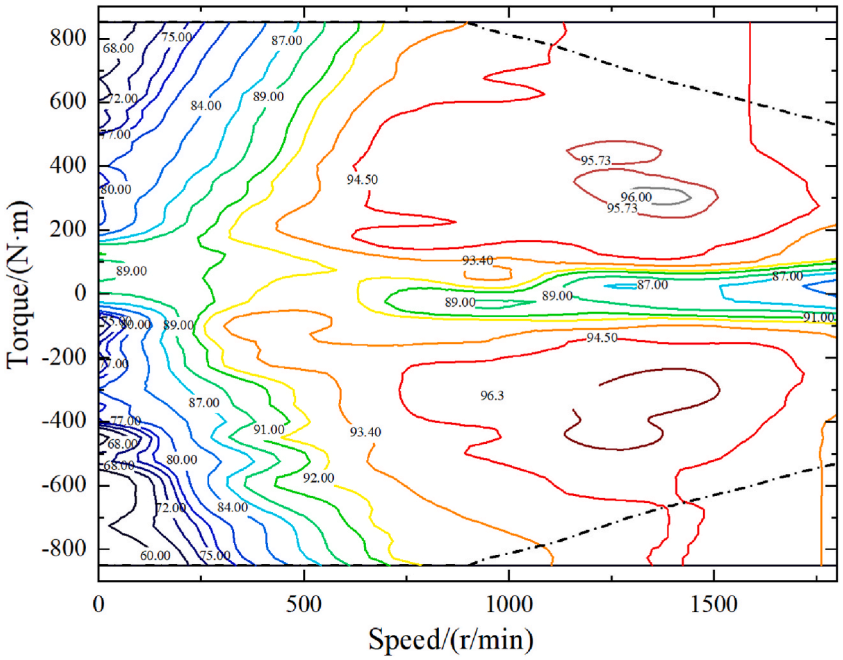

Fig. 5. Efficiency chart.

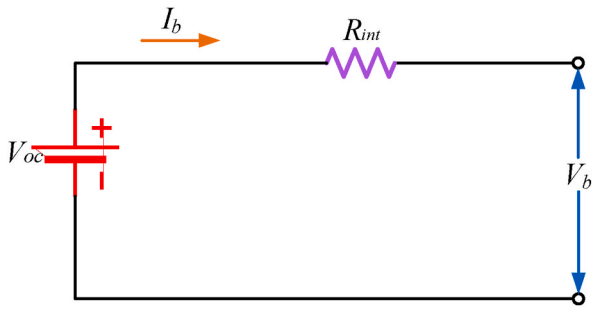

Fig. 6. The equivalent circuit.

3.2. The reversible motor

The reversible motor adopts PI controller. The motor efficiency is mainly obtained by motor torque and speed via the efficiency diagram. The specific design to the function change relationship between the parameters as indicated in Eqs. (16)–(18).

$$n_m = PI(n_{m,target}) \tag{16}$$

$$T_m = \frac{1}{\lambda s + 1} T_{m,target} \tag{17}$$

$$\eta_m = f(n_m, T_m) \tag{18}$$

where $n_{m,target}$ is the target speed of the reversible motor (r/min); n_m is the actual speed of the reversible motor (r/min); PI is the PI controller; $T_{m,target}$ is the input reversible motor target torque (N · m); T_m is the actual output torque of the reversible motor (N · m); η_m is the operating efficiency of the reversible motor, which is obtained by checking the MAP method (%), as illustrated in Fig. 5.

3.3. The energy storage system

The Rint model was chosen to model and simulate the energy storage system [27]. The equivalent circuit is illustrated in Fig. 6. The battery model, which is built upon the Rint equivalent circuit, predominantly explores how parameters V_{oc} and R_{int} change

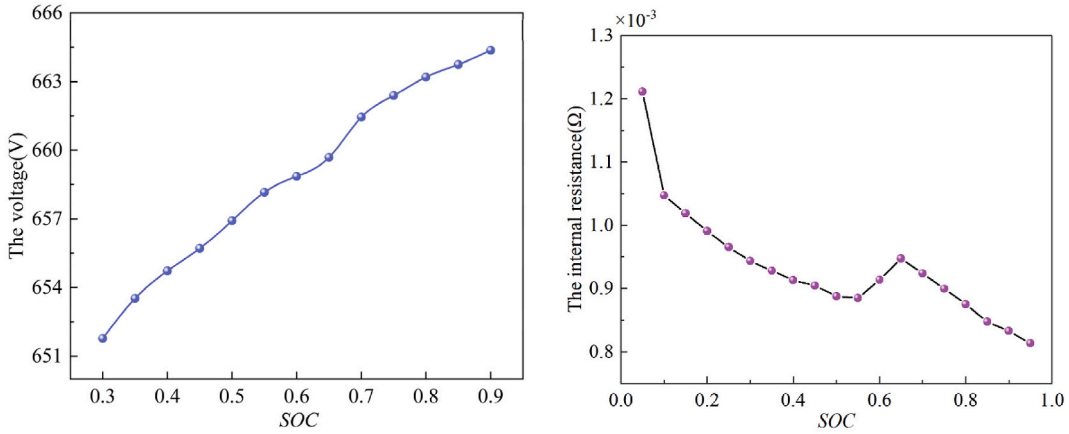

(a) Battery voltage (b) Battery resistance

Fig. 7. The battery voltage and resistance distribution graph.

Table 2
The operating status of devices under different working modes.

Work modes	Sub-mode	Gas engine	Shaft belt generator	Reversible motor	Natural gas generator	Battery
Mechanical Propulsion Modes	Pure Mechanical Propulsion Mode	Work	No work	No work	No work	No work
	Mechanical Propulsion with Reversible Electric Motor Generator Mode	Work	No work	Gene mode	No work	Charging
	Mechanical Propulsion with Reversible Electric Motor Generator Mode II	Work	No work	Gene mode	Work	Charging
	Mechanical Propulsion with Axial Belt Generator Mode	Work	Work	No work	No work	Charging
	Mechanical Propulsion with Axial Belt Generator Mode II	Work	Work	No work	Work	Charging
Electric Propulsion Modes	Gas Engine Electric Propulsion Mode	Work	Work	Motor mode	No work	No work
	Gas Engine Electric Propulsion Mode II	Work	Work	Motor mode	Work	Charging
	Battery Electric Propulsion Mode	No work	No work	Motor mode	No work	Discharging
	Battery Electric Propulsion Mode II	No work	No work	Motor mode	Work	Discharging
	Gas-Electric Hybrid Electric Propulsion Mode	Work	Work	Motor mode	No work	Discharging
	Gas-Electric Hybrid Electric Propulsion Mode II	Work	Work	Motor mode	Work	Discharging
	Electric Propulsion with Axial Belt Generator Auxiliary Power Mode	Work	Work	Motor mode	No work	Charging
	Electric Propulsion with Axial Belt Generator Auxiliary Power Mode II	Work	Work	Motor mode	Work	Charging
	Gas Engine Generator Battery Electric Propulsion Mode	Work	Work	Motor mode	No work	Discharging
	Gas Engine Generator Battery Electric Propulsion Mode II	Work	Work	Motor mode	Work	Discharging
Hybrid Propulsion Modes	Gas-Electric Hybrid Propulsion Mode	Work	No work	Motor mode	No work	Discharging
	Gas-Electric Hybrid Propulsion Mode II	Work	No work	Motor mode	Work	Discharging
	Gas-Electric Hybrid with Axial Belt Generator Auxiliary Power Propulsion Mode	Work	Work	Motor mode	Work	Discharging
	Gas-Electric Hybrid with Axial Belt Generator Auxiliary Power Propulsion Mode II	Work	Work	Motor mode	Work	Discharging
Charging Modes	Gas Engine Generator Charging Mode	Work	Work	No work	No work	Charging
	Gas Engine Generator Charging Mode II	Work	Work	No work	Work	Charging
	Natural Gas Generator Charging Mode	No work	No work	No work	Work	Charging

throughout the battery's operation in response to fluctuations in the battery's State of Charge (SOC), temperature, charge/discharge rates, and other relevant factors [28]. The essential functional relationships within the model are illustrated in Eqs. (19)–(23).

$$V_{oc} = f_{b,\mathrm{oc}}(\mathrm{SOC}) \tag{19}$$

$$R_{\mathrm{int}} = f_{b,R}(\mathrm{SOC}) \tag{20}$$

$$V_b = V_{oc} - I_b R_{\mathrm{int}} \tag{21}$$

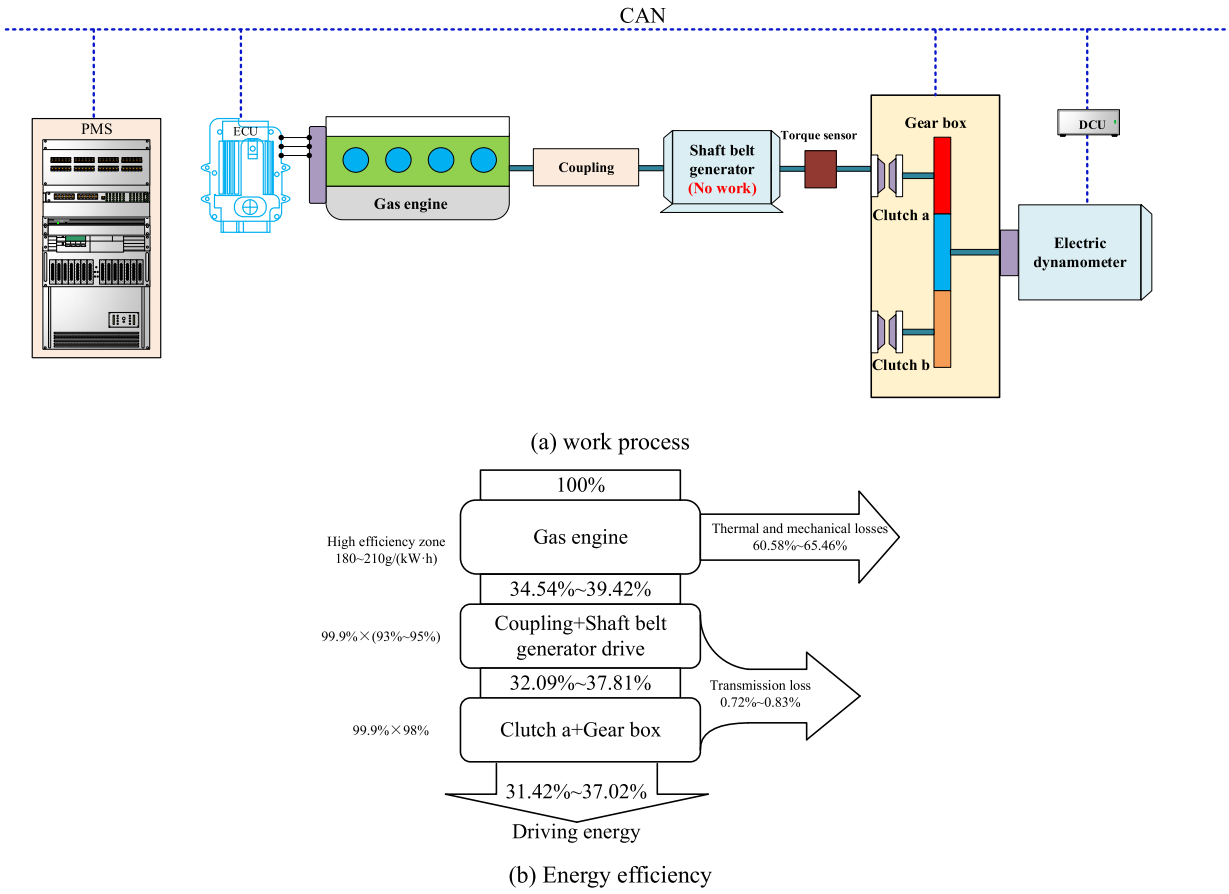

Fig. 8. Pure mechanical propulsion mode.

$$\eta_b = f_{b.eff}(\mathrm{SOC}, T_b) \tag{22}$$

$$\mathrm{SOC}(t) = \mathrm{SOC}(t_0) - \frac{1}{C \times 3600}\int_{t_0}^{t} I_b \eta_b \mathrm{d}t \tag{23}$$

where V_{oc} is the open circuit voltage of the battery (V); $f_{b,\mathrm{oc}}$ is the lookup function of the battery V_{oc} regarding *SOC*; R_{int} is the internal resistance of the battery (Ω); $f_{b,R}$ is the lookup function of the battery R_{int} regarding *SOC*; η_b represents the charging and discharging efficiency of the battery; $f_{b.eff}$ is the lookup function of the battery charging and discharging efficiency regarding *SOC*; T_b is the battery temperature (°C); C is the battery capacity (Ah); SOC(t) is the current battery state of charge; SOC(t_0) is the initial state of charge of the battery.

The distribution of functions V_{oc} and R_{int} with respect to SOC is demonstrated in Fig. 7.

4. Operating modes and energy efficiency

The hybrid gas-electric propulsion modes encompass a diverse range of options, which can be broadly categorized into four main groups: mechanical propulsion, electric propulsion, hybrid propulsion, and charging modes. Here is the specific classification of these propulsion modes:

Mechanical Propulsion Modes: Pure Mechanical Propulsion Mode, Mechanical Propulsion with Reversible Electric Motor Generator Mode, Mechanical Propulsion with Reversible Electric Motor Generator Mode II, Mechanical Propulsion with Axial Belt Generator Mode, Mechanical Propulsion with Axial Belt Generator Mode II.

Electric Propulsion Modes: Gas Engine Electric Propulsion Mode, Gas Engine Electric Propulsion Mode II, Battery Electric Propulsion Mode, Battery Electric Propulsion Mode II, Gas-Electric Hybrid Electric Propulsion Mode, Gas-Electric Hybrid Electric Propulsion Mode II, Electric Propulsion with Axial Belt Generator Auxiliary Power Mode, Electric Propulsion with Axial Belt Generator Auxiliary Power Mode II, Gas Engine Generator Battery Electric Propulsion Mode, Gas Engine Generator Battery Electric Propulsion Mode II.

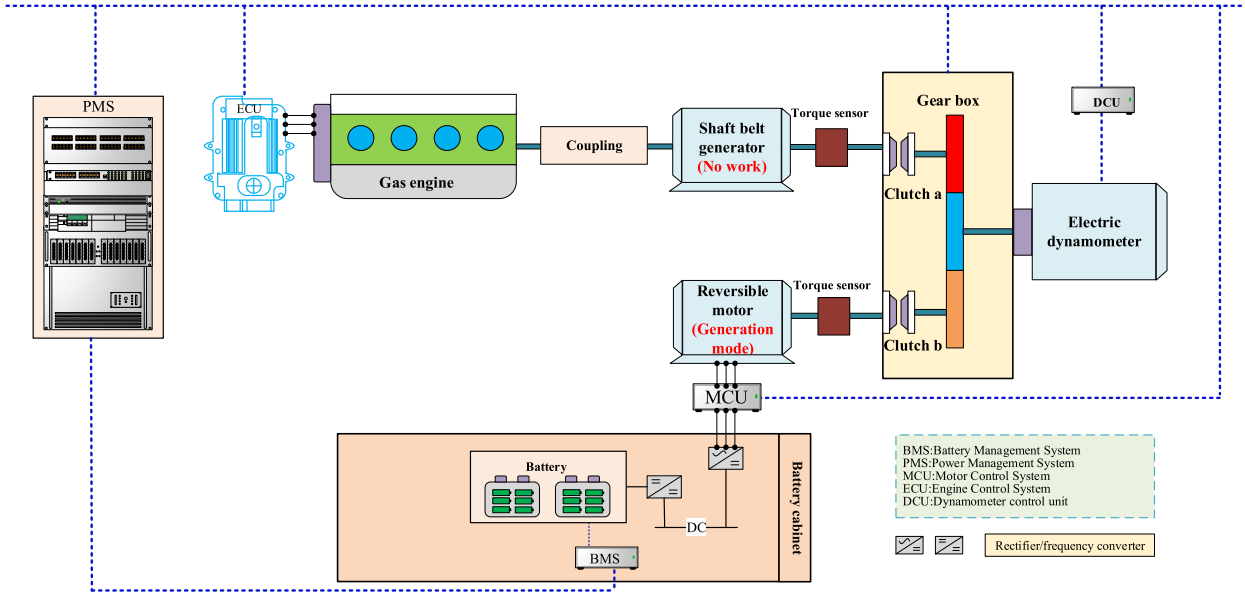

(a) work process

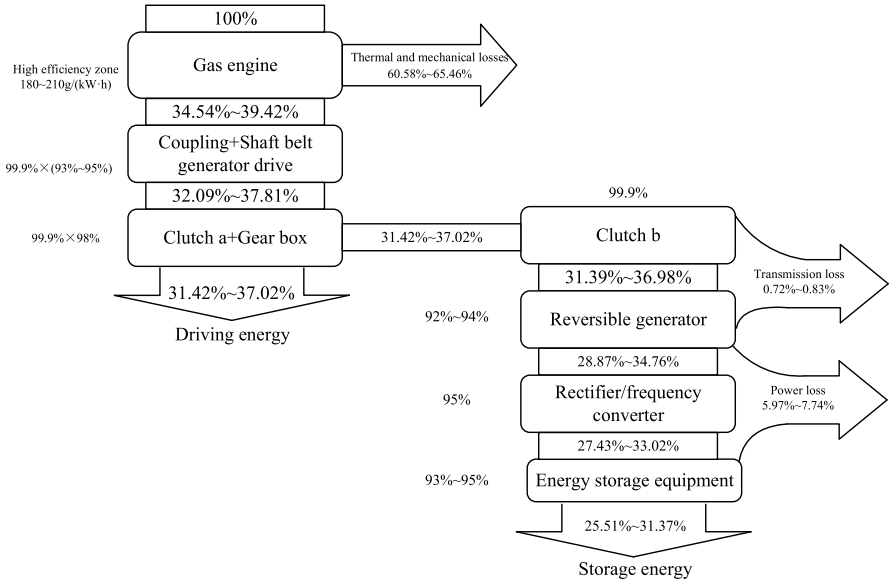

(b) Energy efficiency

Fig. 9. Mechanical propulsion with reversible electric motor generator mode.

Hybrid Propulsion Modes: Gas-Electric Hybrid Propulsion Mode, Gas-Electric Hybrid Propulsion Mode II, Gas-Electric Hybrid with Axial Belt Generator Auxiliary Power Propulsion Mode, Gas-Electric Hybrid with Axial Belt Generator Auxiliary Power Propulsion Mode II.

Charging Modes: Gas Engine Generator Charging Mode, Gas Engine Generator Charging Mode II, Natural Gas Generator Charging Mode.

For a clearer understanding of the operating states of the devices in different operating modes, the operating states of the devices are combed as presented in Table 2.

4.1. Mechanical propulsion modes

Propulsion Mode: Pure Mechanical Propulsion Mode, the operational process is illustrated in Fig. 8(a).

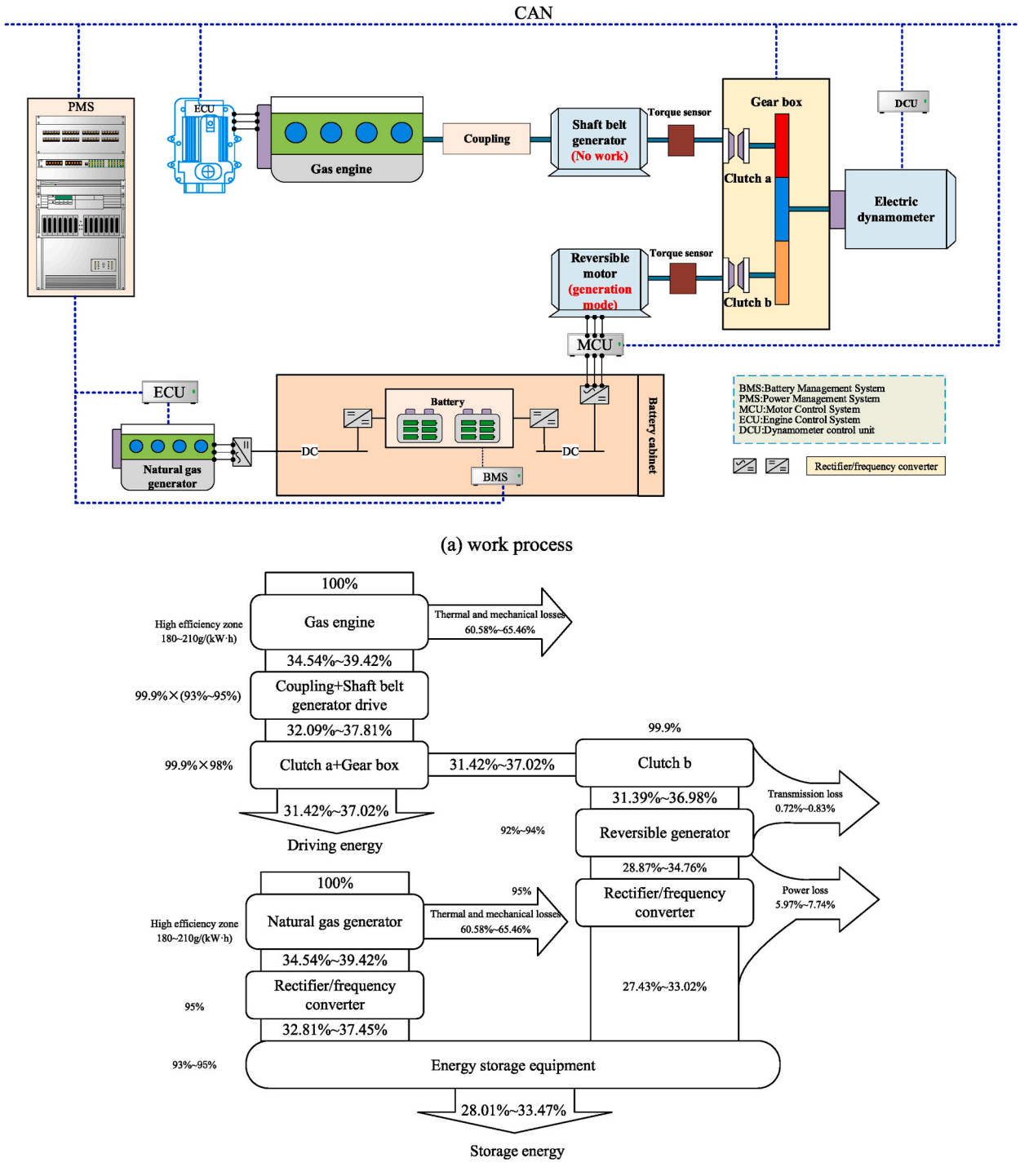

Fig. 10. Mechanical propulsion with reversible electric motor generator mode II.

Status of Components: Gas Engine in Operation, Axial Belt Generator in Shutdown, Natural Gas Engine in Shutdown, Clutch A Closed, Clutch B Open, Energy Storage Device in Shutdown, Reversible Motor in Shutdown, and Electric Dynamometer in Operation.

Energy Flow Path: The entire power output from the gas engine enters the reduction gearbox through clutch A and is fully transferred to the electric dynamometer. The simulated energy efficiency is shown in Fig. 8(b).

Propulsion Mode: Mechanical Propulsion with Reversible Electric Motor Generator Mode.

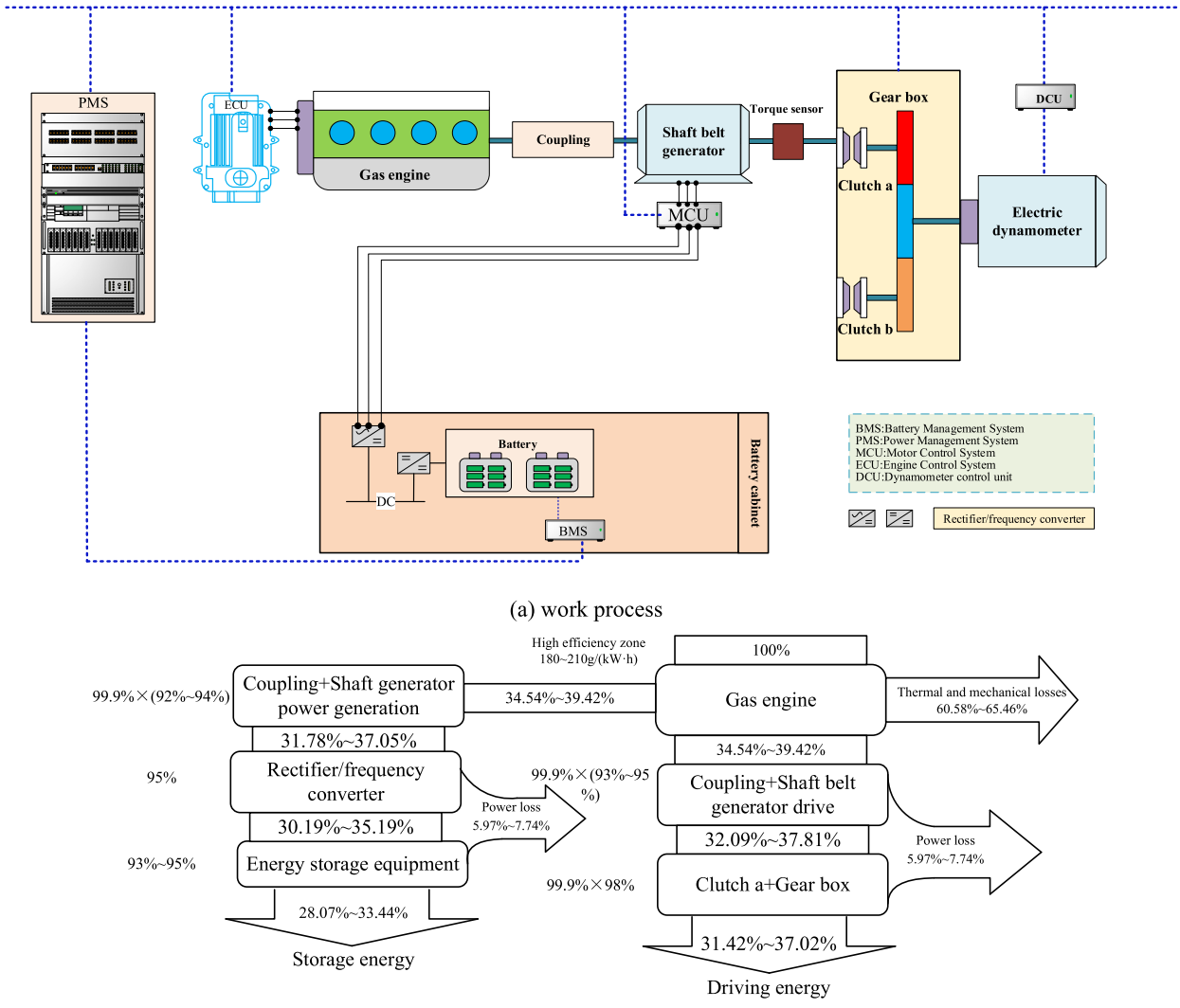

Fig. 11. Mechanical propulsion with shaft belt generator in generator mode.

Status of Components: Gas Engine in Operation, Axial Belt Generator in Shutdown, Natural Gas Generator in Shutdown, Clutch A Closed, Clutch B Closed, Energy Storage Device in Charging Mode, Reversible Motor in Generator Mode, and Electric Dynamometer in Operation. The operational process is illustrated in Fig. 9(a).

Energy Flow Path: The power output from the gas engine enters the reduction gearbox through clutch A, with a portion of the power transferred to the electric dynamometer and another portion passing through clutch B to the reversible motor, where it is converted into electrical energy and stored in the energy storage device. The simulated energy efficiency is shown in Fig. 9(b).

Propulsion Mode: Mechanical Propulsion with Reversible Electric Motor Generator Mode II.

Status of Components: Gas Engine in Operation, Axial Belt Generator in Shutdown, Natural Gas Generator in Operation, Clutch A Closed, Clutch B Closed, Energy Storage Device in Charging Mode, Reversible Motor in Generator Mode, and Electric Dynamometer in Operation. The operational process is illustrated in Fig. 10(a).

Energy Flow Path: The power output from the gas engine enters the reduction gearbox through clutch A, with a portion of the power transferred to the electric dynamometer and another portion passing through clutch B to the reversible motor, where it is converted into electrical energy and stored in the energy storage device. The electrical energy generated by the natural gas generator is also stored in the energy storage device. The simulated energy efficiency is shown in Fig. 10(b).

Propulsion Mode: Mechanical Propulsion with Shaft Belt Generator in Generator Mode.

Status of Components: Gas Engine in Operation, Shaft Belt Generator in Operation, Natural Gas Generator in Shutdown, Clutch A Closed, Clutch B Open, Energy Storage Device in Charging Mode, Reversible Motor in Shutdown, and Electric Dynamometer in Operation. The operational process is illustrated in Fig. 11(a).

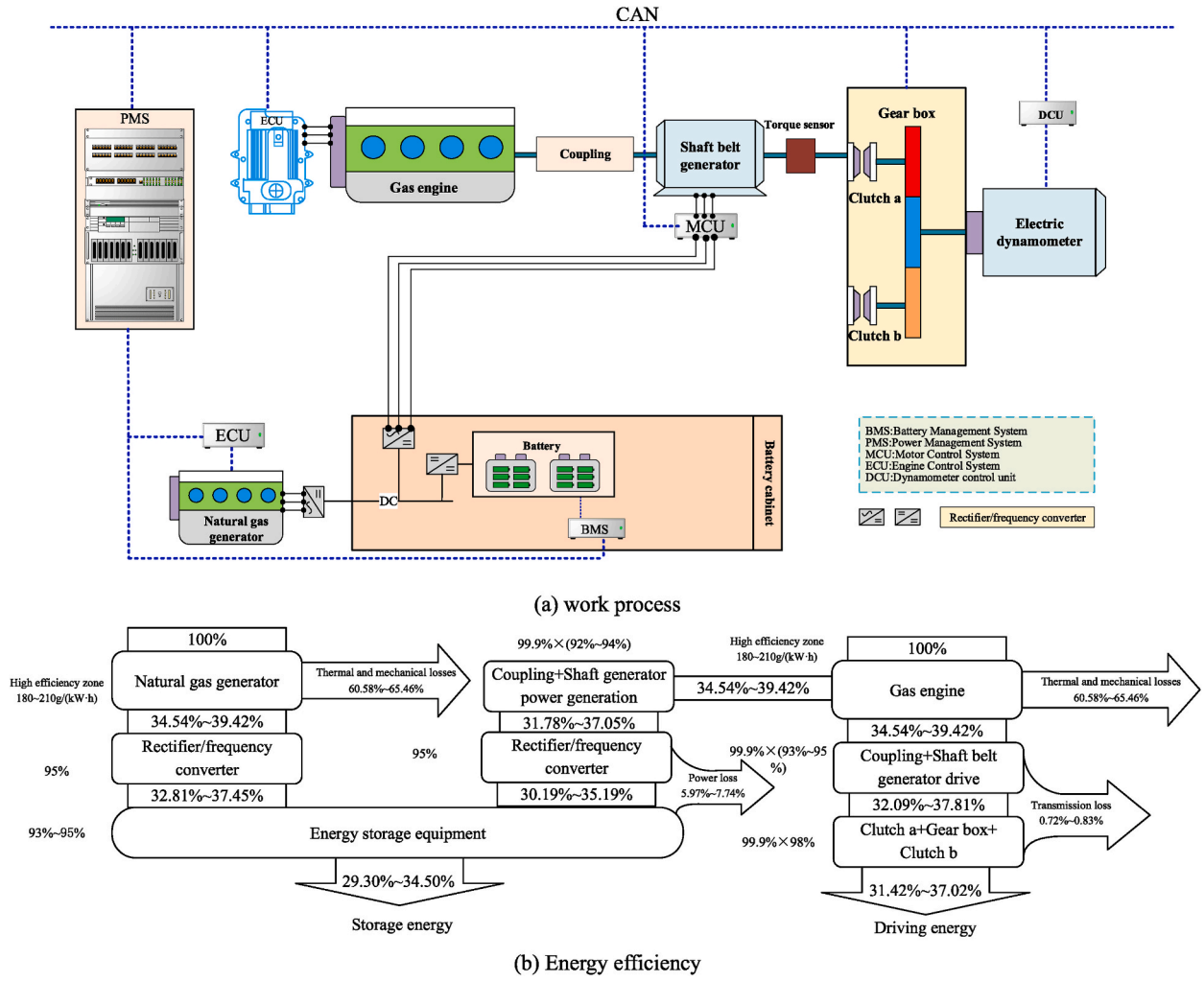

Fig. 12. Mechanical propulsion with shaft belt generator in generator mode II.

Energy Flow Path: Part of the power output from the gas engine enters the reduction gearbox through clutch A and is fully transferred to the electric dynamometer. Another portion of the power is converted into electrical energy by the shaft belt generator and stored in the energy storage device. The simulated energy efficiency is shown in Fig. 11(b).

Propulsion Mode: Mechanical Propulsion with Shaft Belt Generator in Generator Mode II.

Status of Components: Gas Engine in Operation, Shaft Belt Generator in Operation, Natural Gas Generator in Operation, Clutch A Closed, Clutch B Open, Energy Storage Device in Charging Mode, Reversible Motor in Shutdown, and Electric Dynamometer in Operation. The operational process is illustrated in Fig. 12(a).

Energy Flow Path: Part of the power output from the gas engine enters the reduction gearbox through clutch A and is fully transferred to the electric dynamometer. Another portion of the power is converted into electrical energy by the shaft belt generator and stored in the energy storage device, while the electrical energy from the natural gas generator is also stored in the energy storage device. The simulated energy efficiency is shown in Fig. 12(b).

4.2. *Electric propulsion modes*

Propulsion Mode: Gas Engine Electric Propulsion Mode.

Status of Components: Gas Engine in Operation, Shaft Belt Generator in Operation, Clutch A Open, Clutch B Closed, Energy Storage Device in Shutdown Mode, Reversible Motor in Electric Motor Mode, and Electric Dynamometer in Operation. The operational process is illustrated in Fig. 13(a).

Energy Flow Path: The power output from the gas engine is entirely converted into electrical energy by the shaft belt generator and then enters the gearbox through clutch B, passing all of it to the electric dynamometer in the electric motor mode of the reversible motor. The simulated energy efficiency is shown in Fig. 13(b).

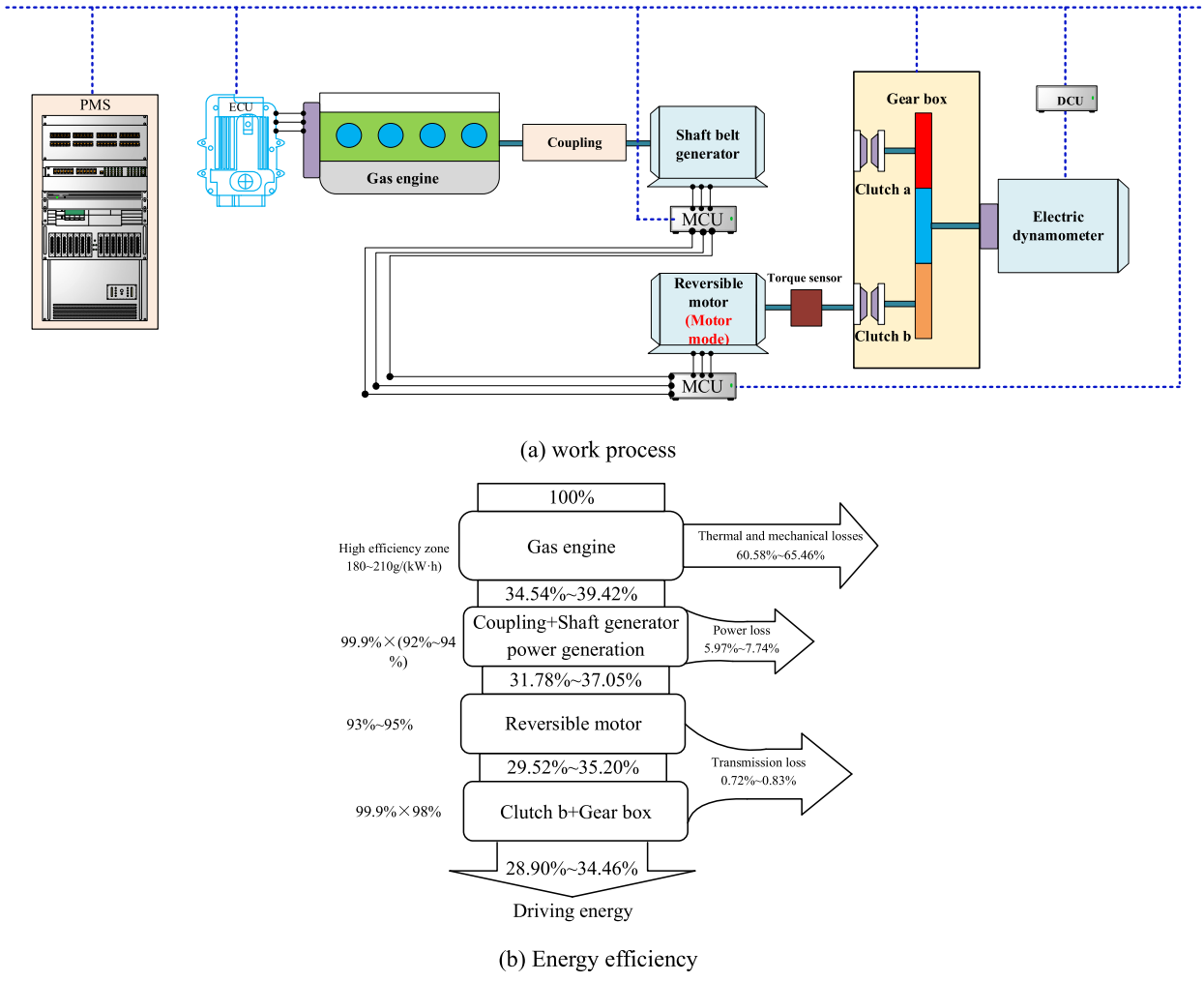

Fig. 13. Gas engine electric propulsion mode.

Propulsion Mode: Gas Engine Electric Propulsion Mode II.

Status of Components: Gas Engine in Operation, Shaft Belt Generator in Operation, Natural Gas Engine in Operation, Clutch A Open, Clutch B Closed, Energy Storage Device in Charging Mode, Reversible Motor in Electric Motor Mode, and Electric Dynamometer in Operation. The operational process is illustrated in Fig. 12(a).

Energy Flow Path: The power output from the gas engine is entirely converted into electrical energy by the shaft belt generator and then enters the gearbox through clutch B, passing all of it to the electric dynamometer in the electric motor mode of the reversible motor. The electrical energy output by the natural gas engine is entirely stored in the energy storage device. The simulated energy efficiency is shown in Fig. 14(b).

Propulsion Mode: Battery Electric Propulsion Mode.

Status of Components: Gas Engine in Shutdown Mode, Shaft Belt Generator in Shutdown Mode, Natural Gas Engine in Shutdown Mode, Clutch A Open, Clutch B Closed, Energy Storage Device in Discharge Mode, Reversible Motor in Electric Motor Mode, and Electric Dynamometer in Operation. The operational process is illustrated in Fig. 15(a).

Energy Flow Path: The energy storage device is in discharge mode, and electrical energy is converted into mechanical energy through the reversible motor, entering the gearbox through clutch B, and then passing it all to the electric dynamometer. The simulated energy efficiency is shown in Fig. 15(b).

Propulsion Mode: Battery Electric Propulsion Mode II.

Status of Components: Gas Engine in Shutdown Mode, Shaft Belt Generator in Shutdown Mode, Natural Gas Engine in Operation, Clutch A Open, Clutch B Closed, Energy Storage Device in Simultaneous Charging and Discharging Mode, Reversible Motor in Electric Motor Mode, and Electric Dynamometer in Operation. The operational process is illustrated in Fig. 16(a).

Energy Flow Path: The energy storage device is in simultaneous charging and discharging mode, electrical energy is converted into mechanical energy through the reversible motor, entering the gearbox through clutch B, and then passing it all to the electric dynamometer. The electrical energy generated by the natural gas engine is all stored in the energy storage system. The simulated

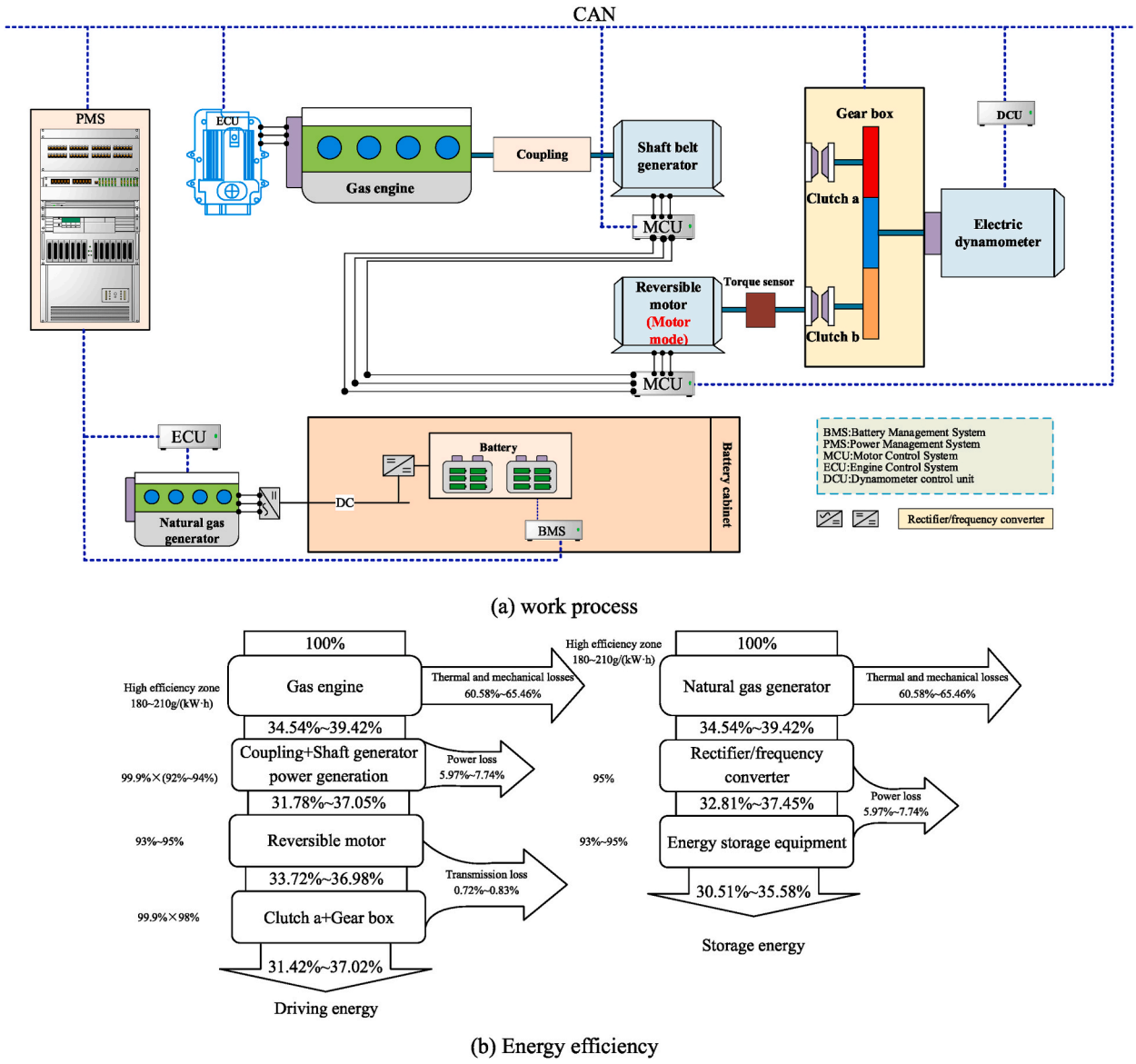

Fig. 14. Gas engine electric propulsion mode II.

energy efficiency is shown in Fig. 16(b).

Propulsion Mode: Gas-Electric Hybrid Electric Propulsion Mode.

Status of Components: Gas Engine in Operation, Shaft Belt Generator in Operation, Natural Gas Engine in Shutdown Mode, Clutch A Open, Clutch B Closed, Energy Storage Device in Discharging Mode, Reversible Motor in Electric Motor Mode, and Electric Dynamometer in Operation. The operational process is illustrated in Fig. 17(a).

Energy Flow Path: The power output from the gas engine is converted into electrical energy through the shaft belt generator, all of which is then input to the reversible motor. The energy storage device releases electrical energy and inputs it to the reversible motor. The electrical energy input to the reversible motor is all converted into mechanical energy, which then enters the gearbox through clutch B and is all passed to the electric dynamometer. The simulated energy efficiency is shown in Fig. 17(b).

Propulsion Mode: Hybrid Electric Power Propulsion Mode II.

Status of Components: Gas Engine in Operation, Shaft Belt Generator in Operation, Natural Gas Engine in Operation, Clutch A Open, Clutch B Closed, Energy Storage Device in Charging and Discharging Mode, Reversible Motor in Electric Motor Mode, and Electric Dynamometer in Operation. The operational process is illustrated in Fig. 18(a).

Energy Flow Path: The power output from the gas engine is converted into electrical energy through the shaft belt generator, all of which is then input to the reversible motor. The energy storage device releases electrical energy and inputs it to the reversible motor. The electrical energy input to the reversible motor is all converted into mechanical energy, which then enters the gearbox through

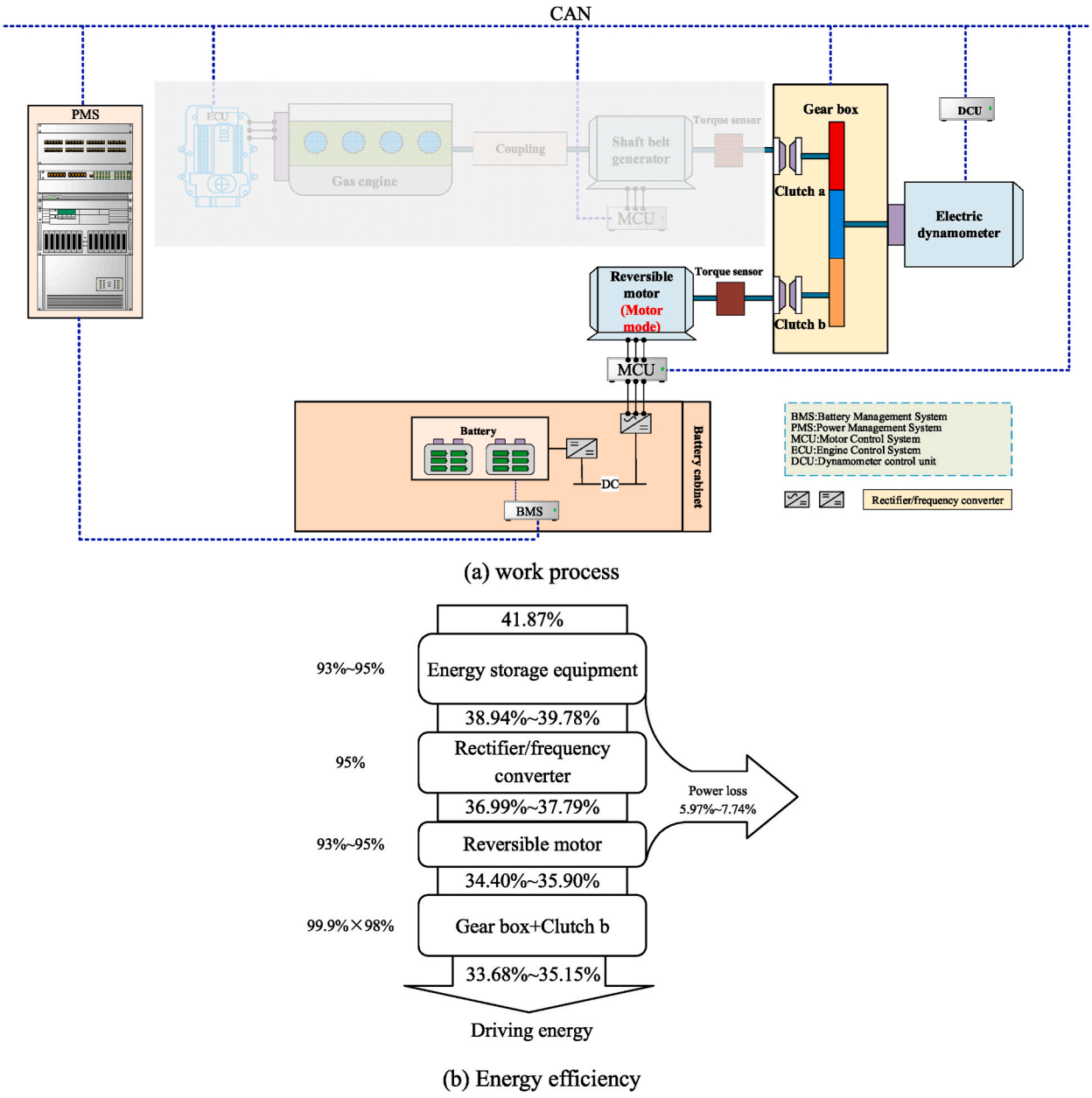

Fig. 15. Battery electric propulsion mode.

clutch B and is all passed to the electric dynamometer. Meanwhile, the electrical energy output by the natural gas generator is all stored in the energy storage device. The simulated energy efficiency is shown in Fig. 18(b).

Propulsion Mode: Electric Propulsion with Axial Belt Generator Auxiliary Power Mode.

Status of Components: Gas Engine in Operation, Shaft Belt Generator in Operation, Natural Gas Engine in Standby, Clutch A Open, Clutch B Closed, Energy Storage Device in Charging Mode, Reversible Motor in Electric Motor Mode, and Electric Dynamometer in Operation. The operational process is illustrated in Fig. 19(a).

Energy Flow Path: The power output from the gas engine is entirely converted into electrical energy through the shaft belt generator. A portion of this electrical energy is stored in the energy storage device, while the other portion is converted into mechanical energy through the reversible motor. The mechanical energy then enters the gearbox through clutch B and is entirely passed to the electric dynamometer. The simulated energy efficiency is shown in Fig. 19(b).

Propulsion Mode: Electric Propulsion with Axial Belt Generator Auxiliary Power Mode II.

Status of Components: Gas Engine in Operation, Shaft Belt Generator in Operation, Natural Gas Engine in Operation, Clutch A Open, Clutch B Closed, Energy Storage Device in Charging Mode, Reversible Motor in Electric Motor Mode, and Electric Dynamometer

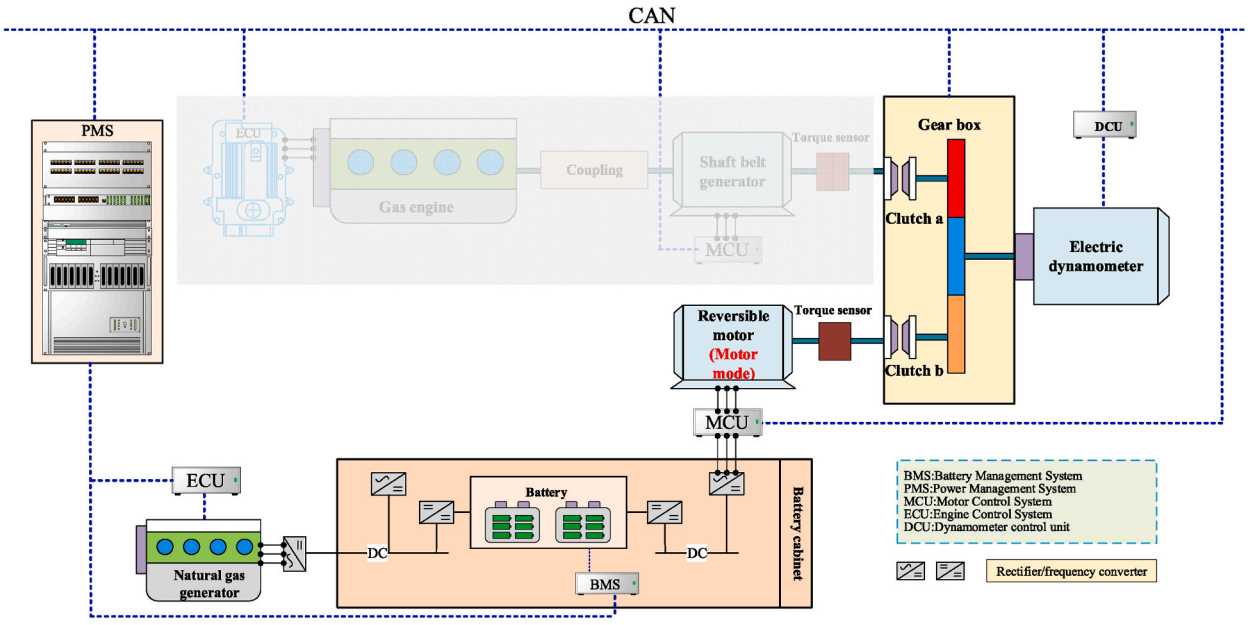

(a) work process

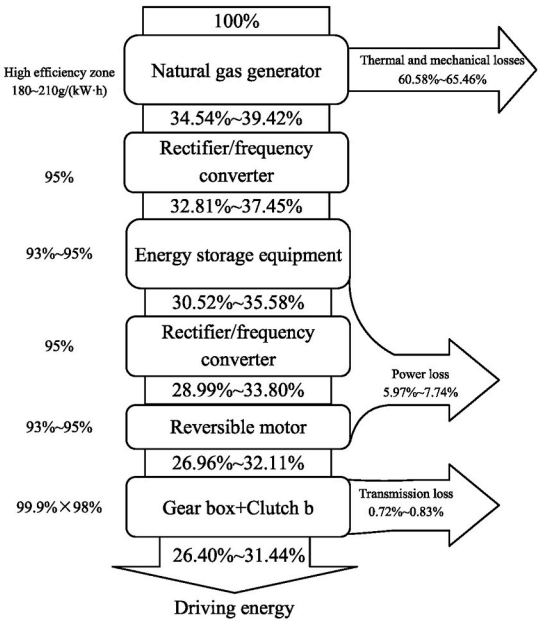

(b) Energy efficiency

Fig. 16. Battery electric propulsion mode II.

in Operation. The operational process is illustrated in Fig. 20(a).

Energy Flow Path: The power output from the gas engine is entirely converted into electrical energy through the shaft belt generator. A portion of this electrical energy is stored in the energy storage device, while the other portion is converted into mechanical energy through the reversible motor. The mechanical energy then enters the gearbox through clutch B and is entirely passed to the electric dynamometer. Additionally, all the electrical energy output from the natural gas engine is stored in the energy storage device. The simulated energy efficiency is shown in Fig. 20(b).

Propulsion Mode: Gas Engine Electric Battery Electric Propulsion Mode.

Status of Components: Gas Engine in Operation, Shaft Belt Generator in Operation, Natural Gas Engine in Shutdown Mode, Clutch A

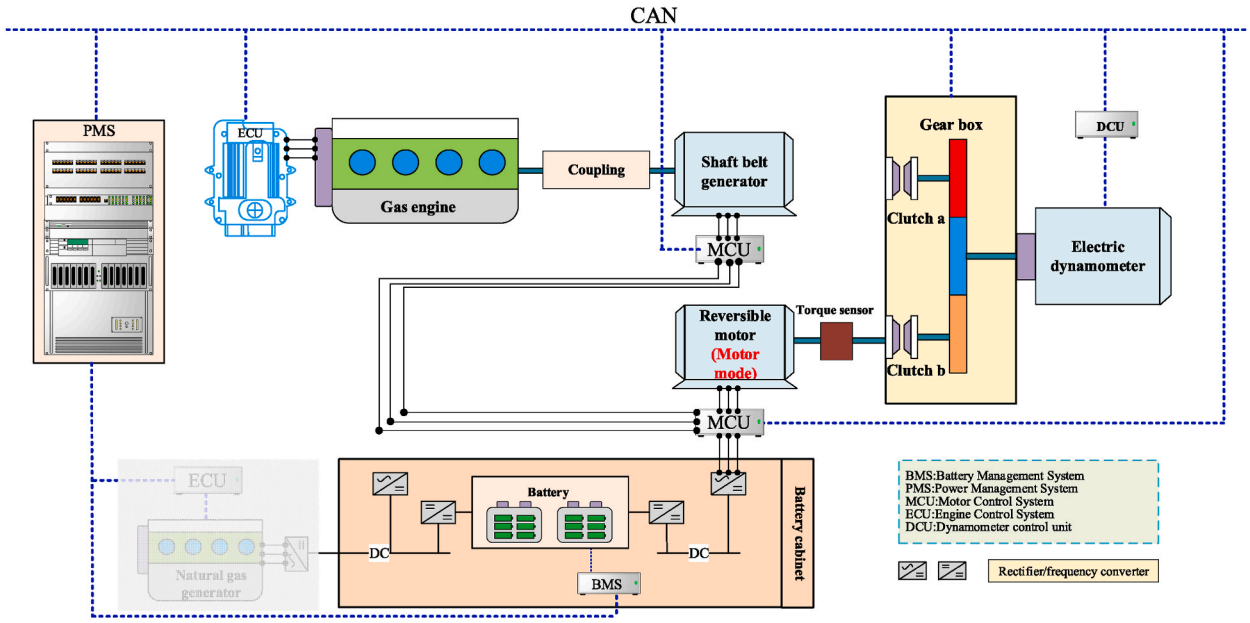

(a) work process

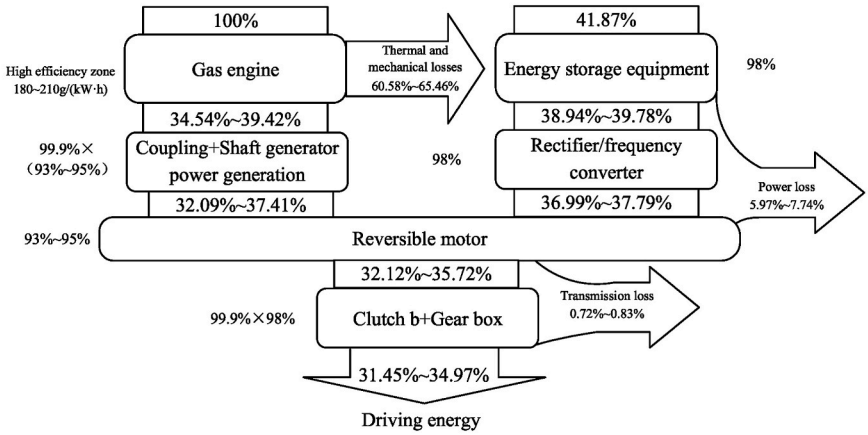

(b) Energy efficiency

Fig. 17. Gas-electric hybrid electric propulsion mode.

Open, Clutch B Closed, Energy Storage Device in Both Charging and Discharging Mode, Reversible Motor in Electric Motor Mode, and Electric Dynamometer in Operation. The operational process is illustrated in Fig. 21(a).

Energy Flow Path: The power output from the gas engine is entirely converted into electrical energy through the shaft belt generator, which is then stored in the energy storage device. The energy storage device is in both charging and discharging mode, releasing electrical energy that is then converted into mechanical energy through the reversible motor. The mechanical energy enters the gearbox through clutch B and is entirely passed to the electric dynamometer. The simulated energy efficiency is shown in Fig. 21 (b).

Propulsion Mode: Gas Engine Electric Battery Electric Propulsion Mode II.

Status of Components: Gas Engine in Operation, Shaft Belt Generator in Operation, Natural Gas Engine in Operation, Clutch A Open, Clutch B Closed, Energy Storage Device in Both Charging and Discharging Mode, Reversible Motor in Electric Motor Mode, and Electric Dynamometer in Operation. The operational process is illustrated in Fig. 22(a).

Energy Flow Path: The power output from the gas engine is entirely converted into electrical energy through the shaft belt generator, which is then stored in the energy storage device. The energy storage device is in both charging and discharging mode, releasing electrical energy that is then converted into mechanical energy through the reversible motor. The mechanical energy enters

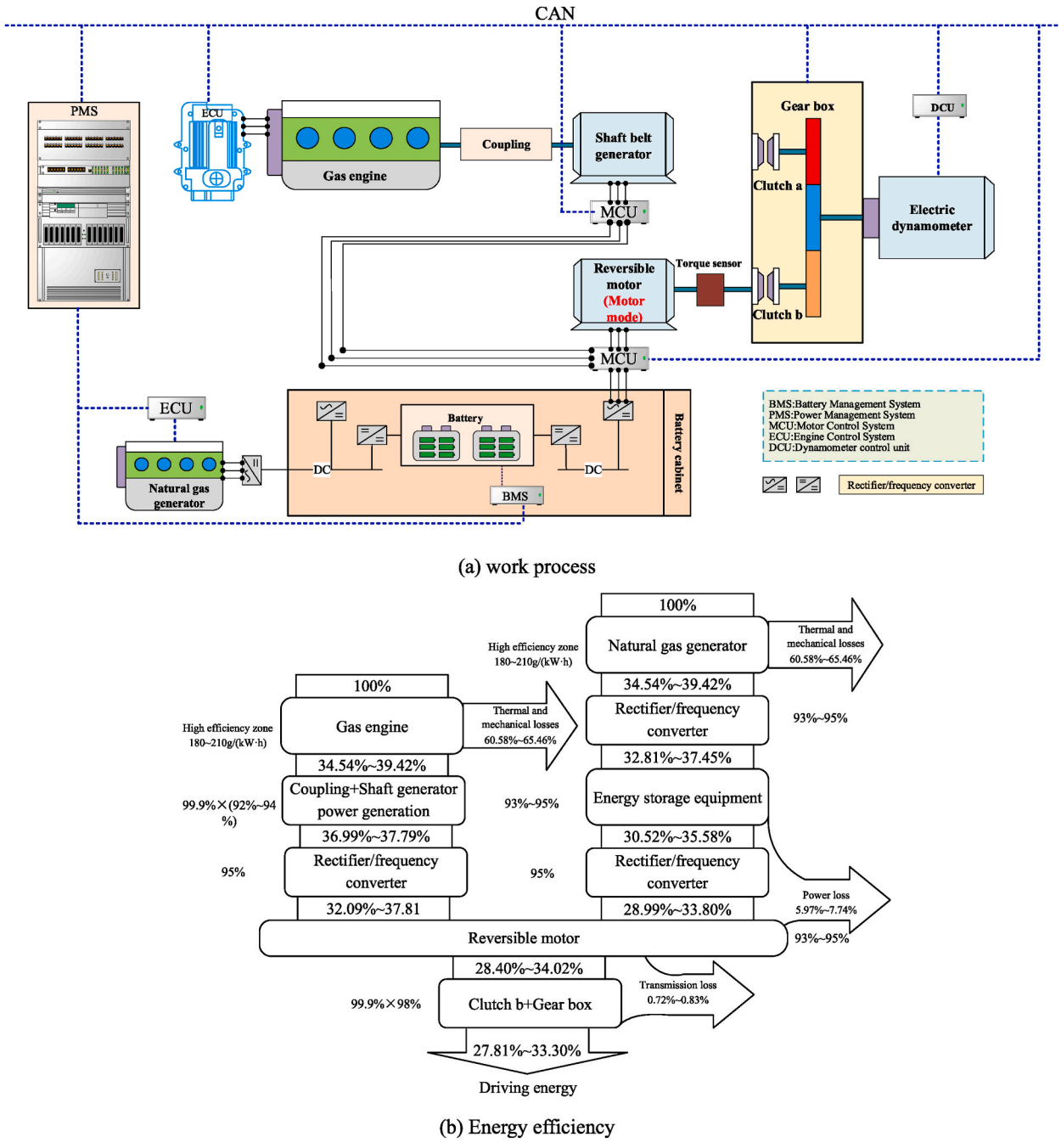

Fig. 18. Gas-electric hybrid electric propulsion mode II.

the gearbox through clutch B and is entirely passed to the electric dynamometer. Simultaneously, the electrical energy generated by the natural gas engine is stored in the energy storage device. The simulated energy efficiency is shown in Fig. 22(b).

4.3. Hybrid propulsion

Propulsion Mode: Gas-Electric Hybrid Propulsion Mode.

Status of Components: Gas Engine in Operation, Shaft Belt Generator in Standby Mode, Natural Gas Engine in Standby Mode, Clutch A Closed, Clutch B Closed, Energy Storage Device in Discharging Mode, Reversible Motor in Electric Motor Mode, and Electric Dynamometer in Operation. The operational process is illustrated in Fig. 23(a).

Energy Flow Path: The power output from the gas engine enters the gearbox through clutch A. The energy storage device is in

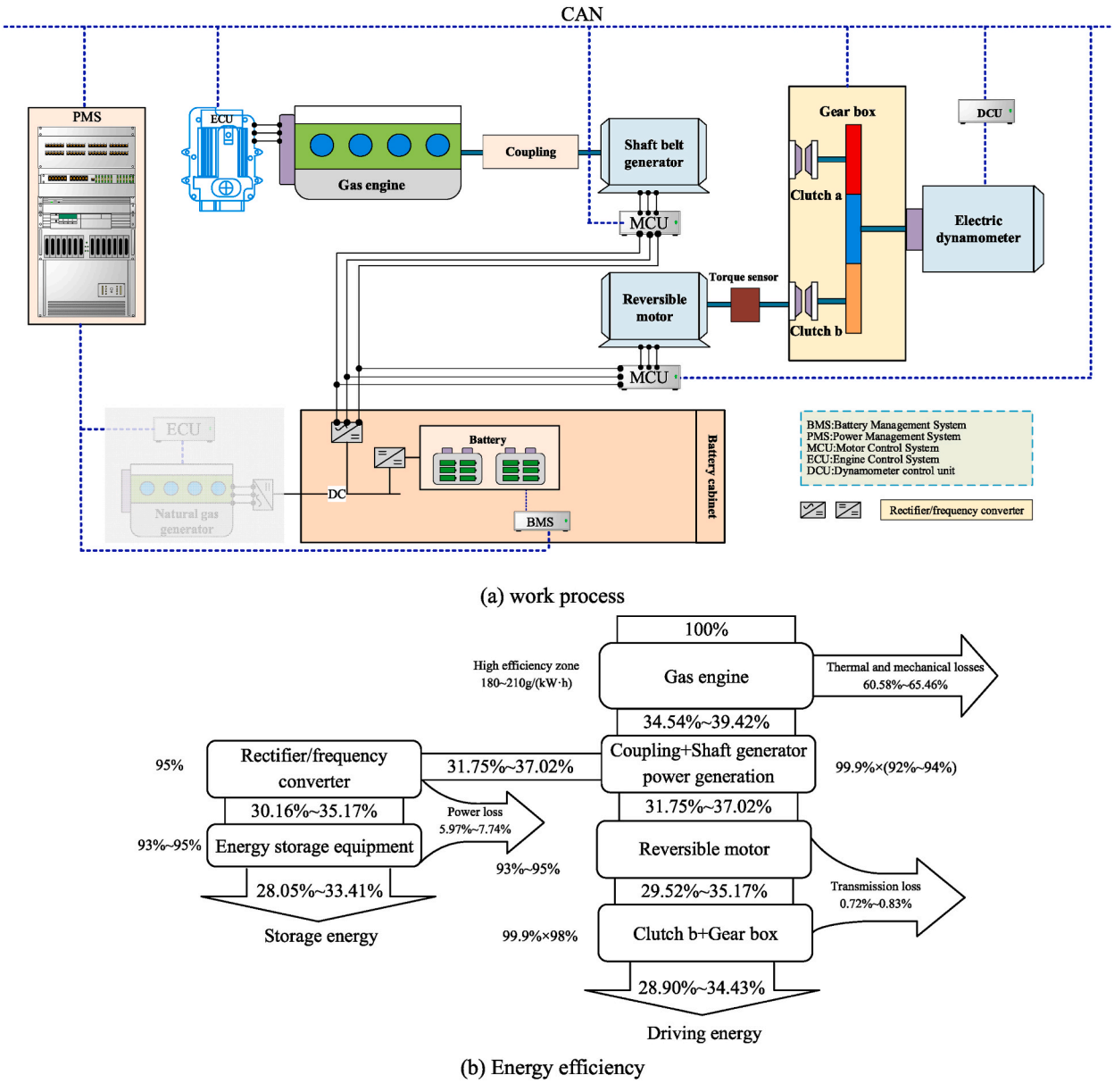

Fig. 19. Electric propulsion with Axial belt generator auxiliary power mode.

discharging mode, releasing electrical energy that is then converted into mechanical energy through the reversible motor. The mechanical energy enters the gearbox through clutch B. All the mechanical energy entering the gearbox through clutch A and clutch B is then transmitted to the electric dynamometer. Simulated energy efficiency is shown in Fig. 23(b).

Propulsion Mode: Gas-Electric Hybrid Propulsion Mode II.

Status of Components: Gas Engine in Operation, Shaft Belt Generator in Standby Mode, Natural Gas Engine in Operation, Clutch A Closed, Clutch B Closed, Energy Storage Device in Simultaneous Charging and Discharging Mode, Reversible Motor in Electric Motor Mode, and Electric Dynamometer in Operation. The operational process is illustrated in Fig. 24(a).

Energy Flow Path: The power output from the gas engine enters the gearbox through clutch A. The energy storage device is simultaneously in charging and discharging mode, releasing electrical energy that is then converted into mechanical energy through the reversible motor. The mechanical energy enters the gearbox through clutch B. All the mechanical energy entering the gearbox through clutch A and clutch B is then transmitted to the electric dynamometer. Additionally, all the electrical energy output from the natural gas engine is stored in the energy storage device. Simulated energy efficiency is shown in Fig. 24(b).

Propulsion Mode: Gas-Electric Hybrid with Axial Belt Generator Auxiliary Power Propulsion Mode.

Status of Components: Gas Engine in Operation, Shaft Belt Generator in Operation, Natural Gas Engine in Standby Mode, Clutch A

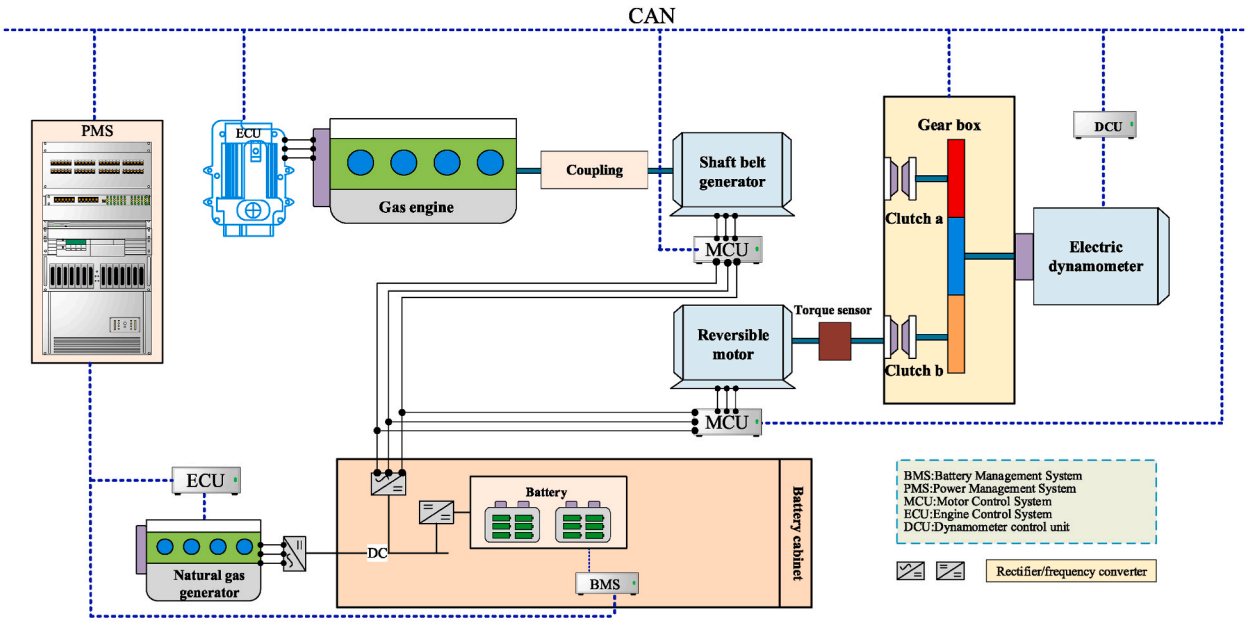

(a) work process

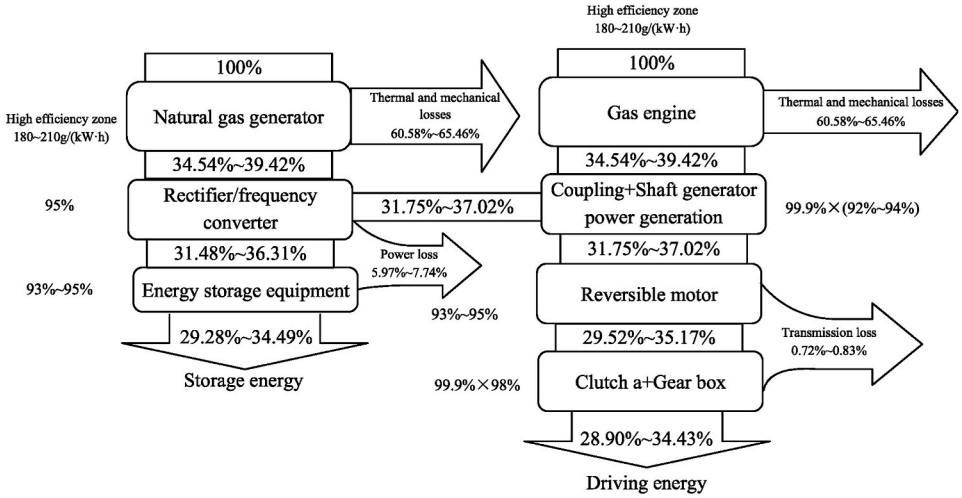

(b) Energy efficiency

Fig. 20. Electric propulsion with Axial belt generator auxiliary power mode II.

Closed, Clutch B Closed, Energy Storage Device in Simultaneous Charging and Discharging Mode, Reversible Motor in Electric Motor Mode, and Electric Dynamometer in Operation. The operational process is illustrated in Fig. 25(a).

Energy Flow Path: A portion of the power output from the gas engine is converted into electrical energy through the shaft belt generator and stored in the energy storage device. Another portion of the energy enters the gearbox through clutch A. The energy storage device is simultaneously in charging and discharging mode, releasing electrical energy that is then converted into mechanical energy through the reversible motor. The mechanical energy enters the gearbox through clutch B. All the mechanical energy entering the gearbox through clutch A and clutch B is then transmitted to the electric dynamometer. Simulated energy efficiency is shown in Fig. 25(b).

Propulsion Mode: Gas-Electric Hybrid with Axial Belt Generator Auxiliary Power Propulsion Mode II.

Status of Components: Gas Engine in Operation, Shaft Belt Generator in Operation, Natural Gas Engine in Operation, Clutch A Closed, Clutch B Closed, Energy Storage Device in Simultaneous Charging and Discharging Mode, Reversible Motor in Electric Motor Mode, and Electric Dynamometer in Operation. The operational process is illustrated in Fig. 26(a).

Energy Flow Path: A portion of the power output from the gas engine is converted into electrical energy through the shaft belt

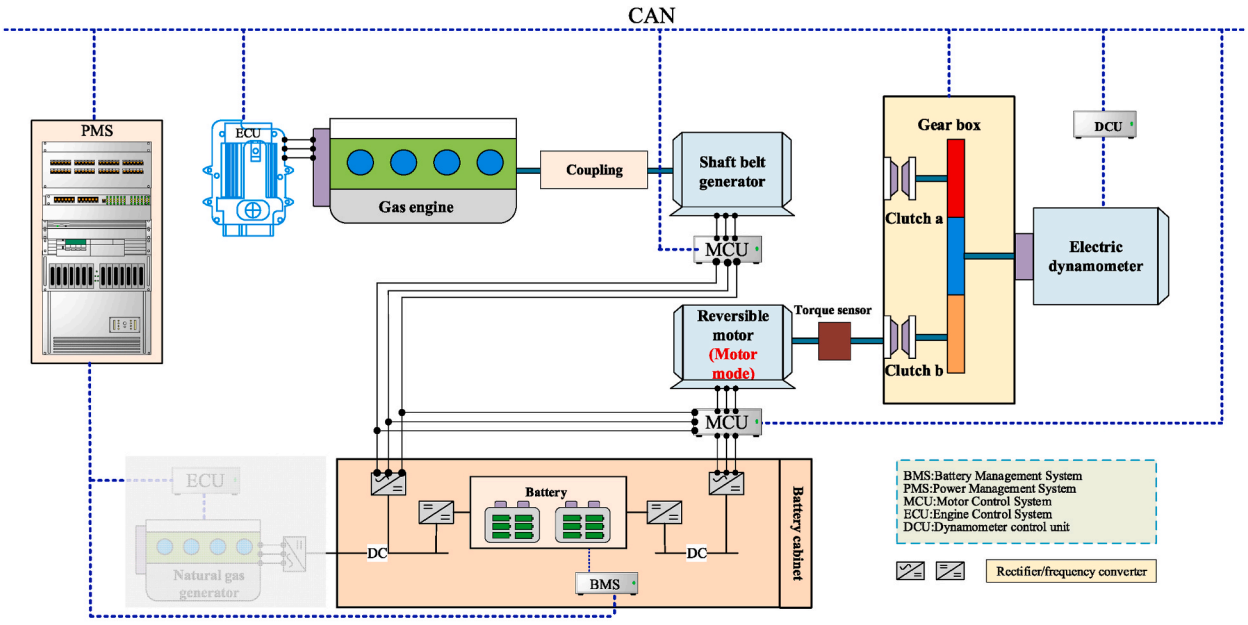

(a) work process

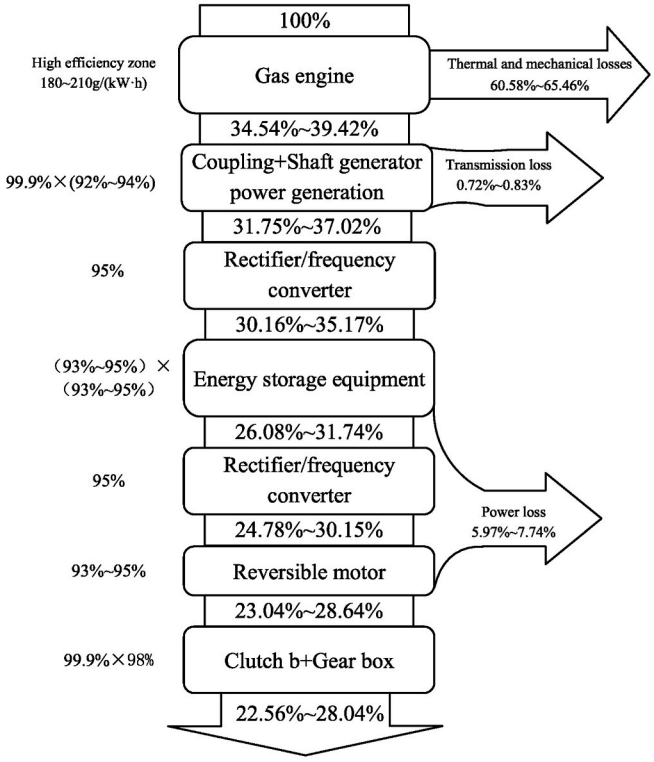

(b) Energy efficiency

Fig. 21. Gas engine electric battery electric propulsion mode.

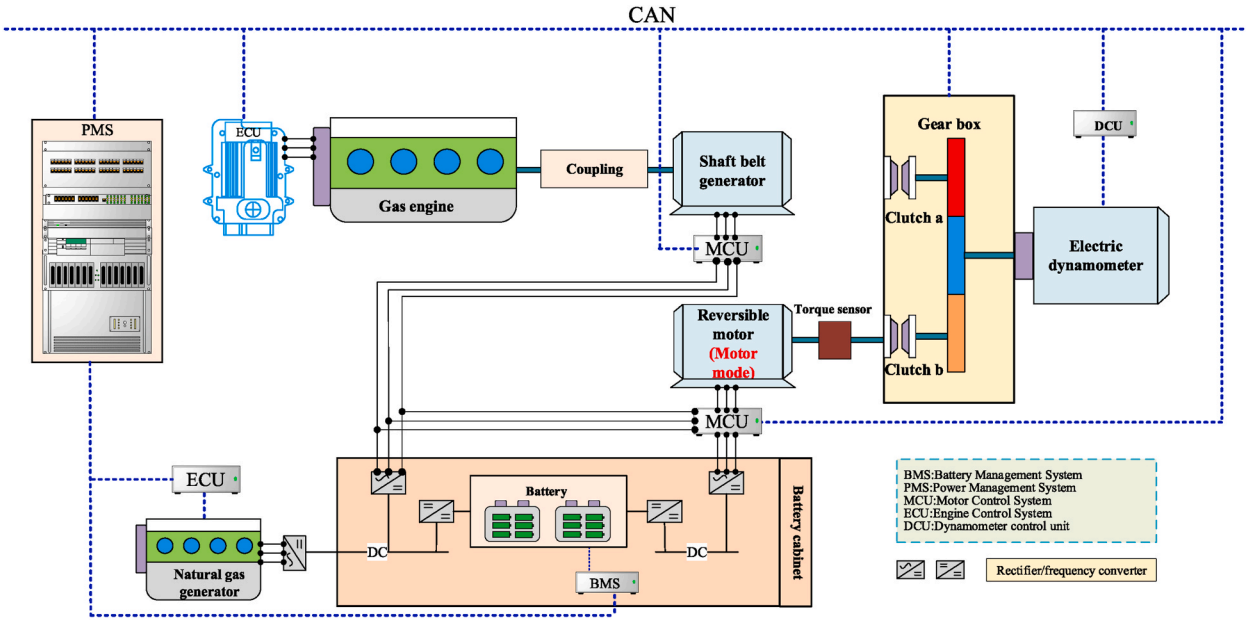

(a) work process

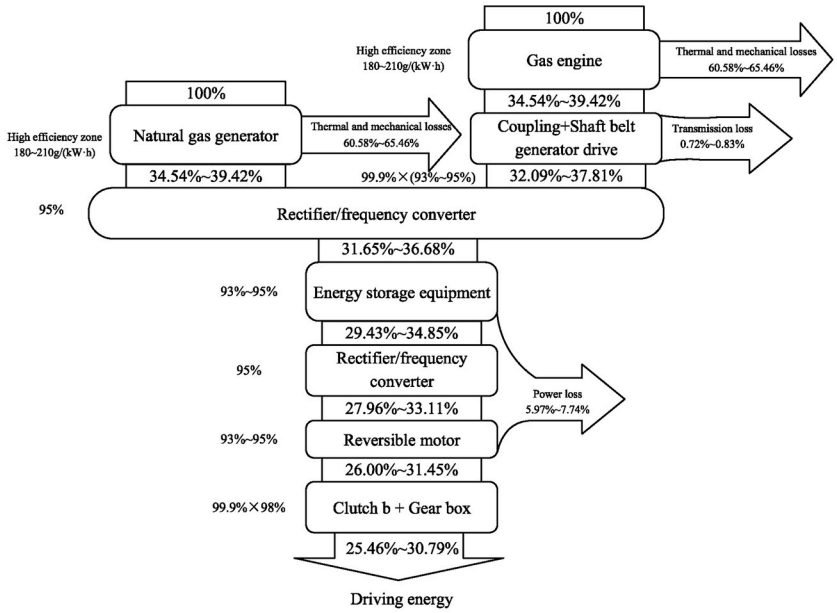

(b) Energy efficiency

Fig. 22. Gas engine electric battery electric propulsion mode II.

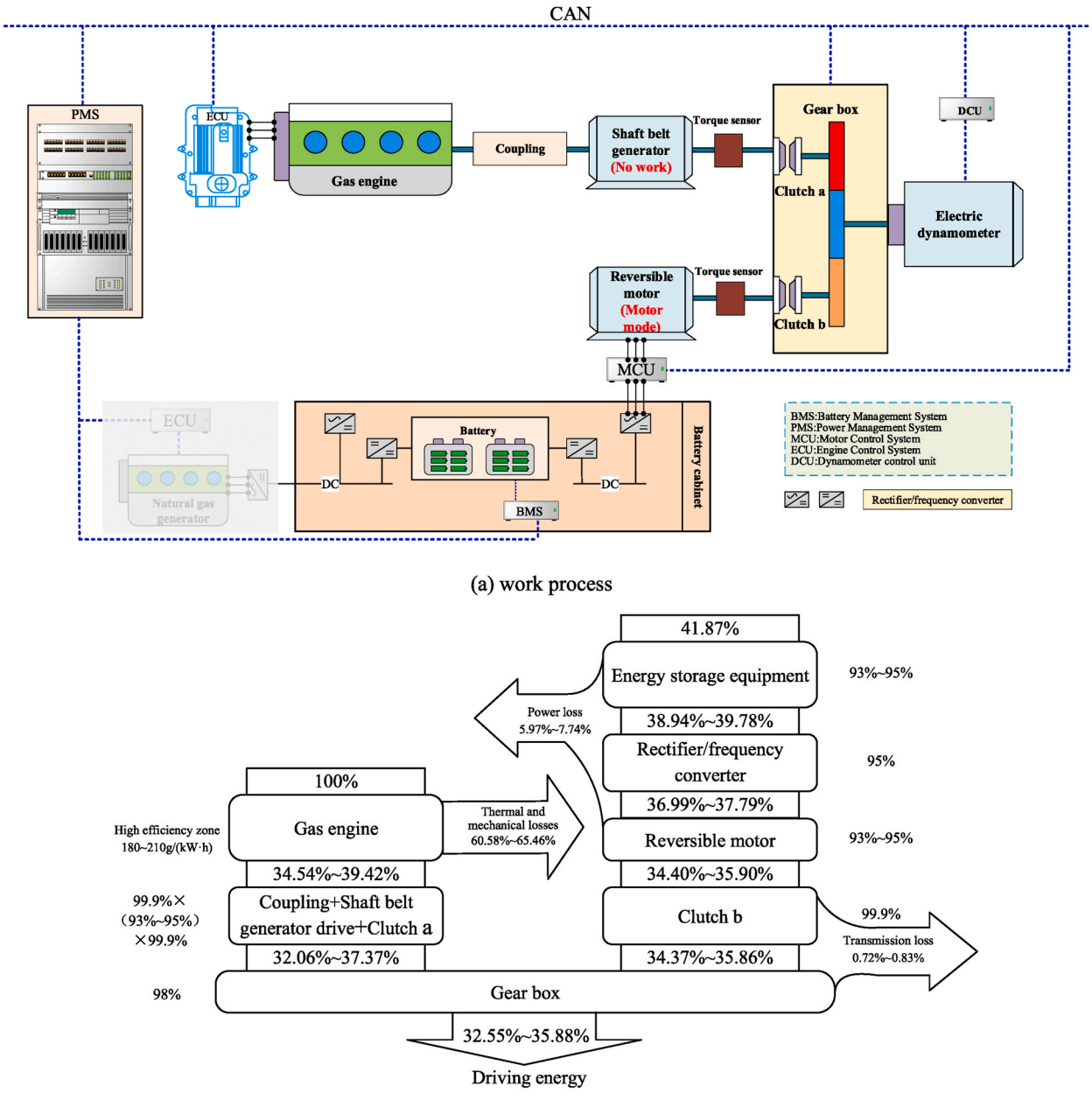

Fig. 23. Gas-electric hybrid propulsion mode.

generator and stored in the energy storage device. Another portion of the energy enters the gearbox through clutch A. The energy storage device is simultaneously in charging and discharging mode, releasing electrical energy that is then converted into mechanical energy through the reversible motor. The mechanical energy enters the gearbox through clutch B. All the mechanical energy entering the gearbox through clutch A and clutch B is then transmitted to the electric dynamometer. At the same time, the electrical energy output from the natural gas generator is stored in the energy storage device. Simulated energy efficiency is shown in Fig. 26(b).

4.4. Charging modes

Propulsion Mode: Gas Engine Generator Charging Mode.

Status of Components: Gas Engine in Operation, Shaft Belt Generator in Operation, Natural Gas Engine in Shutdown, Clutch A Open, Clutch B Open, Energy Storage Device in Charging Mode, Reversible Motor in Shutdown Mode, and Electric Dynamometer in

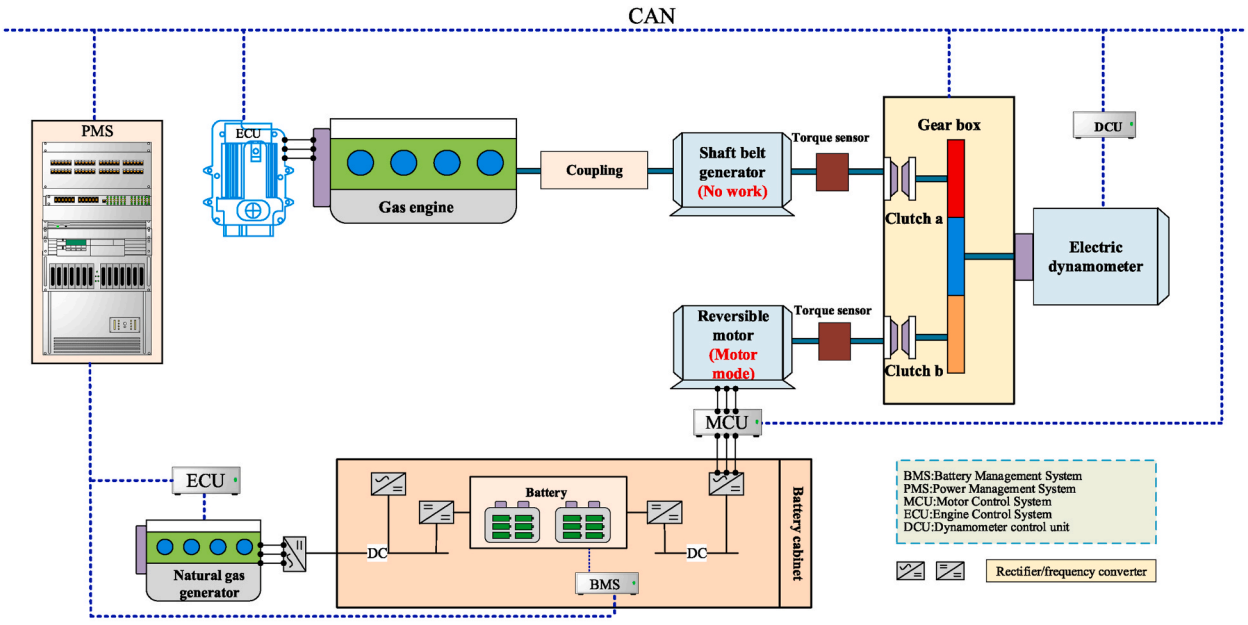

(a) work process

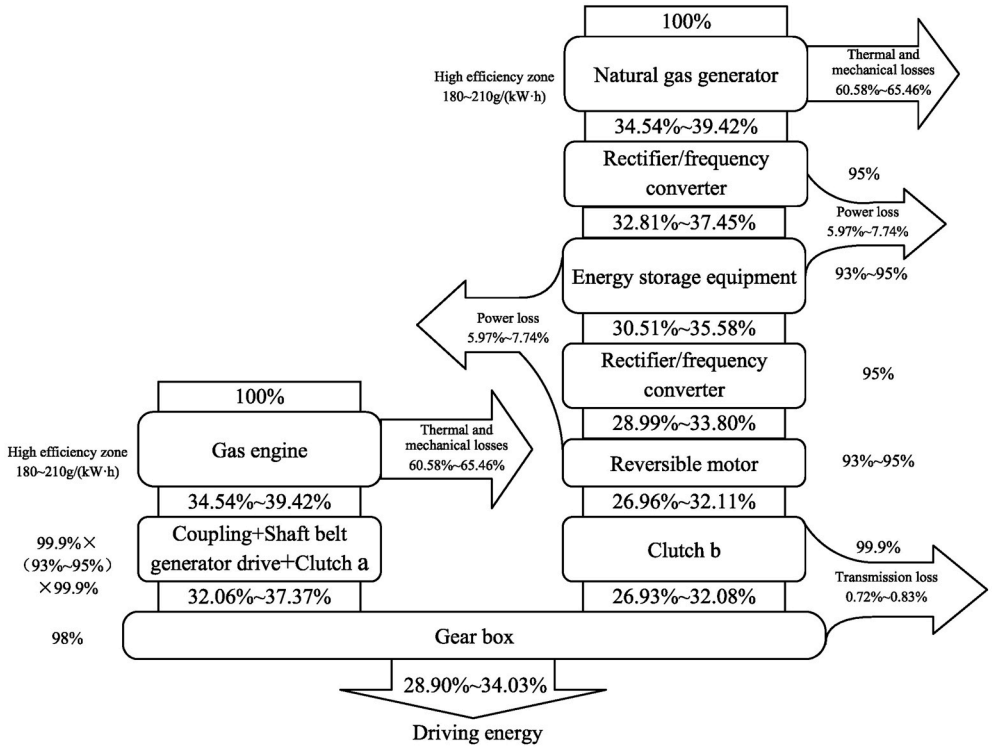

(b) Energy efficiency

Fig. 24. Gas-electric hybrid propulsion mode II.

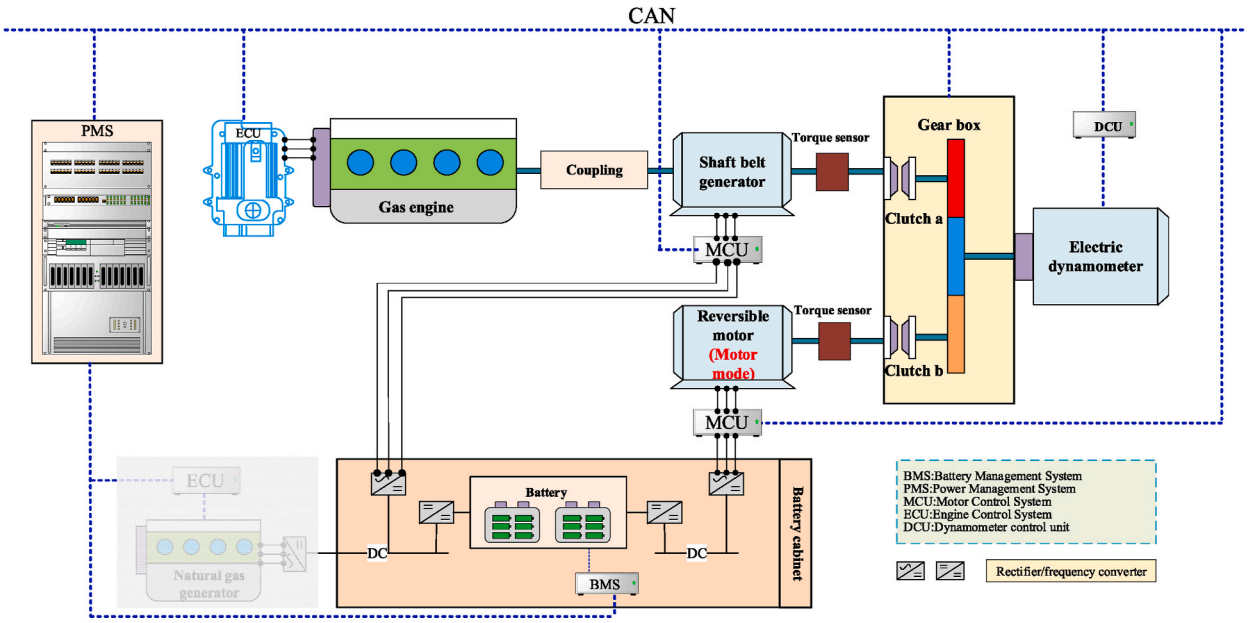

(a) work process

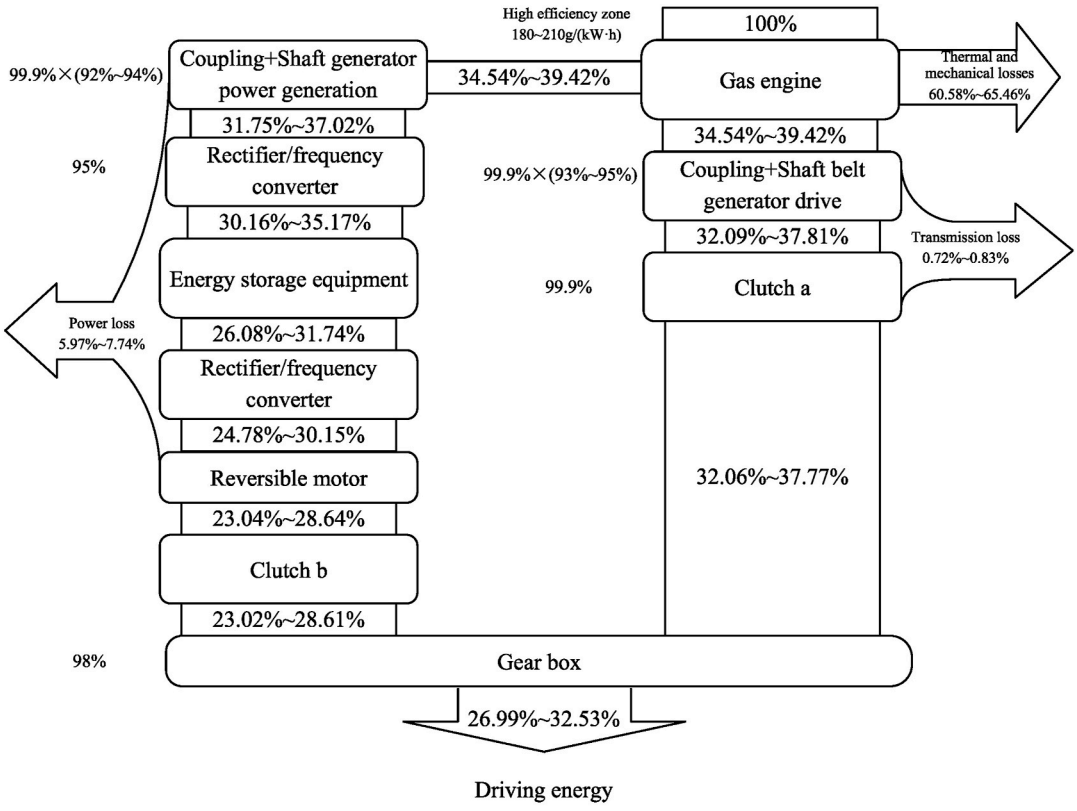

(b) Energy efficiency

Fig. 25. Gas-electric hybrid with Axial belt generator auxiliary power propulsion mode.

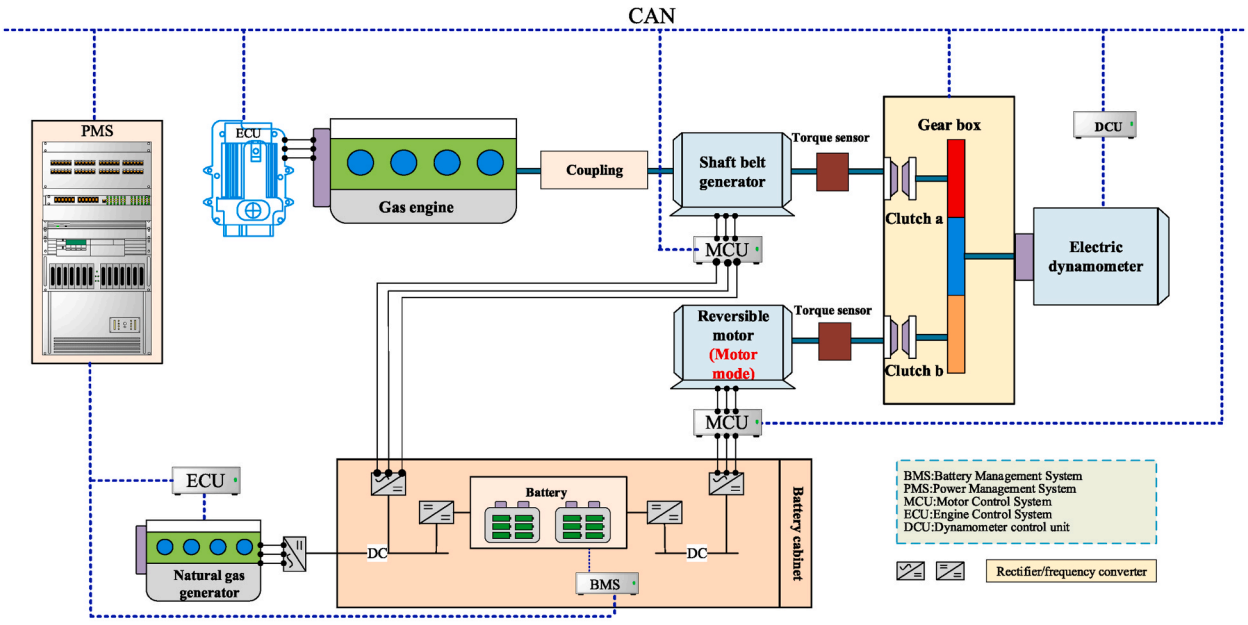

(a) work process

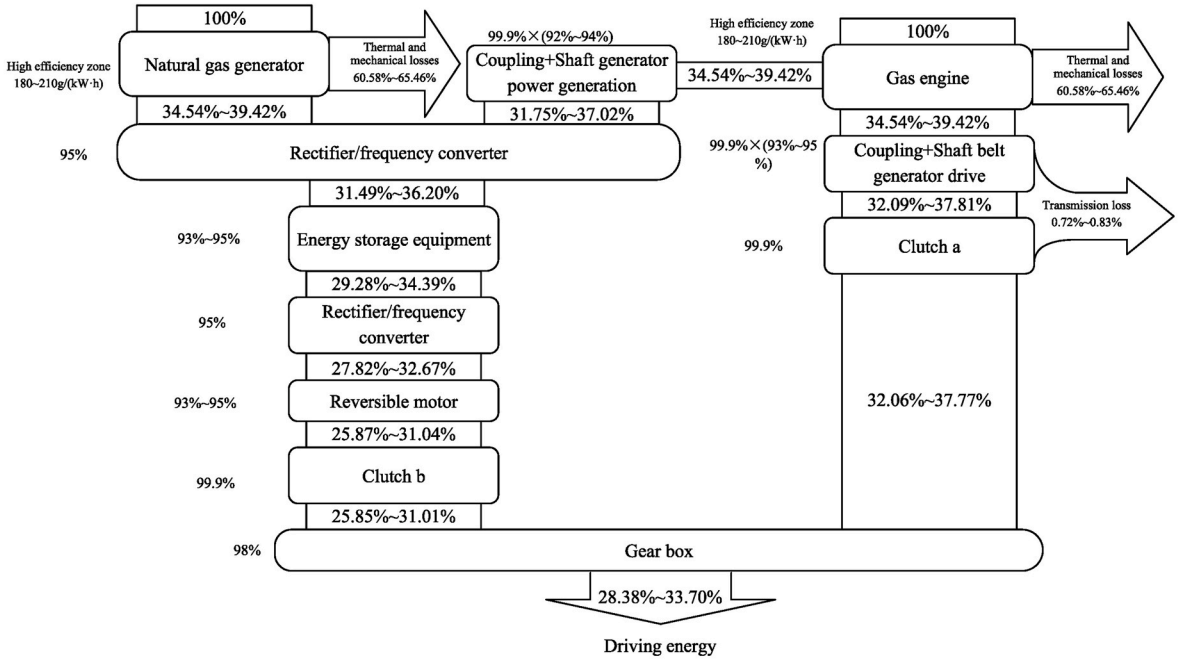

(b) Energy efficiency

Fig. 26. Gas-electric hybrid with Axial belt generator auxiliary power propulsion mode II.

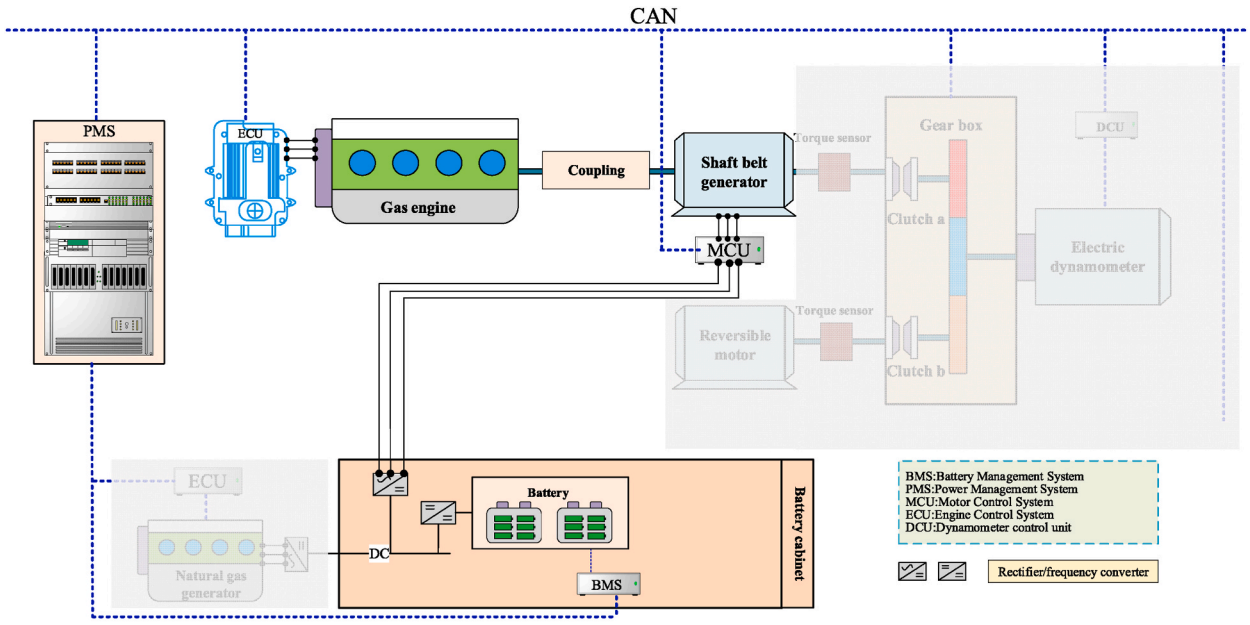

(a) work process

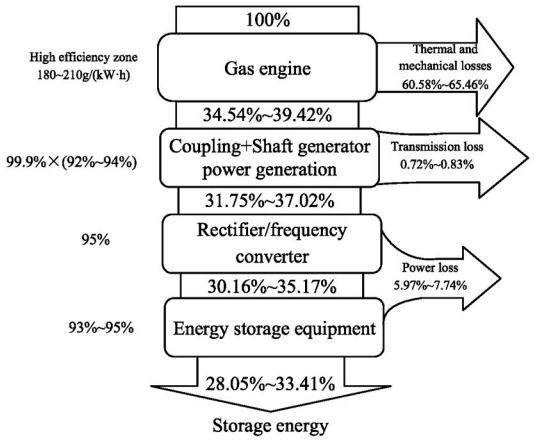

(b) Energy efficiency

Fig. 27. Gas engine generator charging mode.

Shutdown Mode. The operational process is illustrated in Fig. 27(a).

Energy Flow Path: The power output from the gas engine is entirely converted into electrical energy through the shaft belt generator and stored entirely in the energy storage device, which is in charging mode. Simulated energy efficiency is shown in Fig. 27 (b).

Propulsion Mode: Gas Engine Generator Charging Mode II.

Status of Components: Gas Engine in Operation, Shaft Belt Generator in Operation, Natural Gas Engine in Operation, Clutch A Open, Clutch B Open, Energy Storage Device in Charging Mode, Reversible Motor in Shutdown Mode, and Electric Dynamometer in Shutdown Mode. The operational process is illustrated in Fig. 28(a).

Energy Flow Path: The power output from the gas engine is entirely converted into electrical energy through the shaft belt generator and stored entirely in the energy storage device, which is in charging mode. Simultaneously, the electrical energy generated by the natural gas engine is entirely stored in the energy storage device. Simulated energy efficiency is shown in Fig. 28(b).

Propulsion Mode: Natural Gas Generator Charging Mode.

Status of Components: Gas Engine in Shutdown Mode, Shaft Belt Generator in Shutdown Mode, Natural Gas Engine in Operation, Clutch A Open, Clutch B Open, Energy Storage Device in Charging Mode, Reversible Motor in Shutdown Mode, and Electric Dynamometer in Shutdown/Operational Mode. The operational process is illustrated in Fig. 29(a).

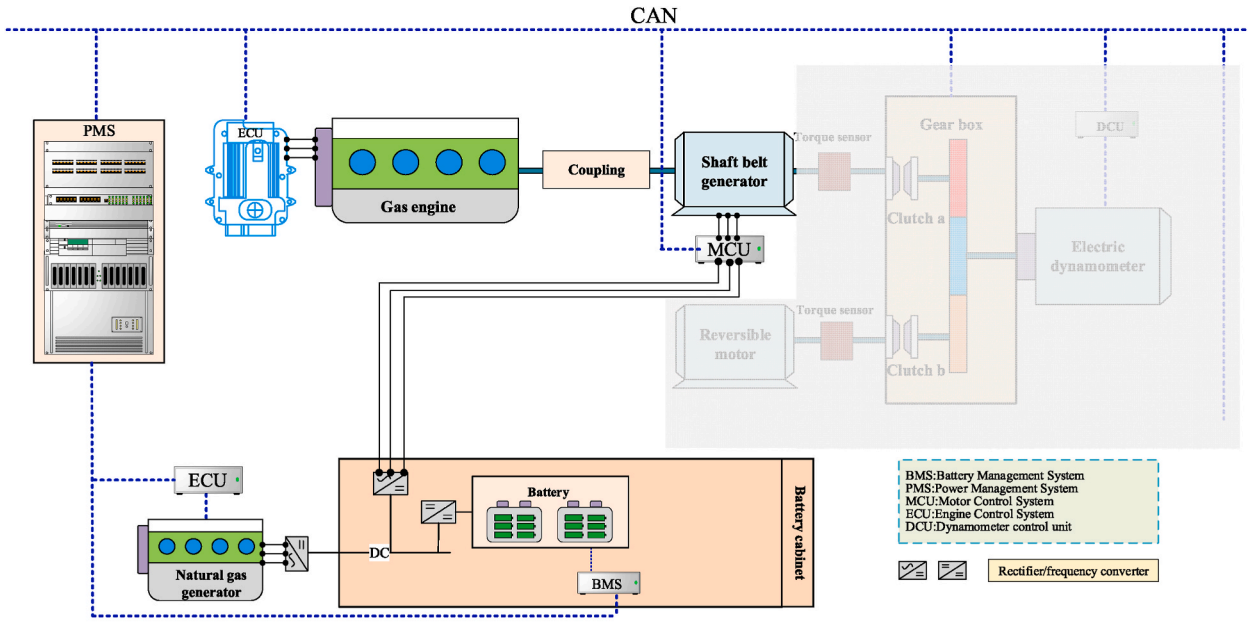

(a) work process

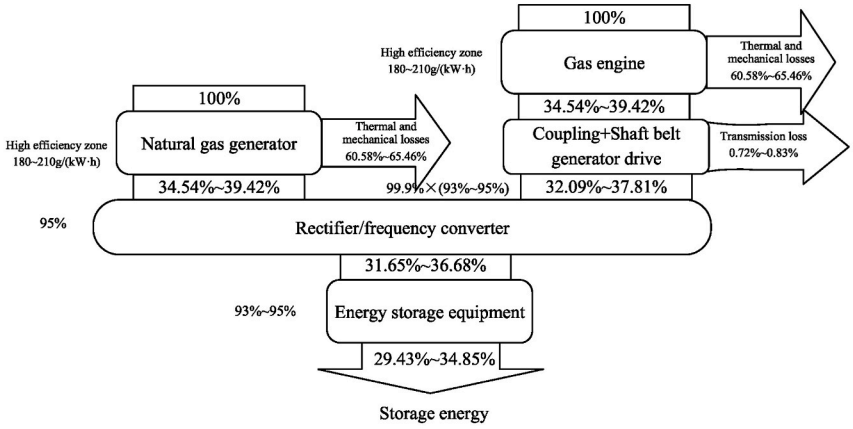

(b) Energy efficiency

Fig. 28. Gas engine generator charging mode II.

Energy Flow Path: The electrical energy generated by the natural gas engine is entirely stored in the energy storage device, which is in charging mode. Simulated energy efficiency is shown in Fig. 29(b).

Table 3 provides a comprehensive summary of energy efficiency in various modes, and it yields several key conclusions that offer significant guidance for the design and performance optimization of hybrid gas-electric propulsion systems:

Natural Gas Engine Dominance: The natural gas engine consistently exhibits outstanding energy efficiency in various propulsion modes, reaching a maximum of up to 37.02 %. This highlights the pivotal role played by the natural gas engine within the propulsion system, particularly excelling in high-efficiency mechanical propulsion modes.

Mechanical Propulsion Efficiency: Mechanical propulsion modes display a notable energy efficiency range, spanning from 31.42 % to 37.02 %. This suggests that mechanical propulsion can provide relatively efficient power transmission across diverse operating conditions.

Electric Propulsion Variation: Energy efficiency within electric propulsion modes exhibits considerable variability across different scenarios. Notably, the battery-powered electric propulsion mode demonstrates the least variation, ranging from 33.68 % to 35.15 %. Overall, electric propulsion modes offer relatively high energy efficiency but display inconsistent performance under varying conditions.

Hybrid Propulsion Modes: Hybrid propulsion modes showcase a broad range of energy efficiency, with the gas-electric hybrid

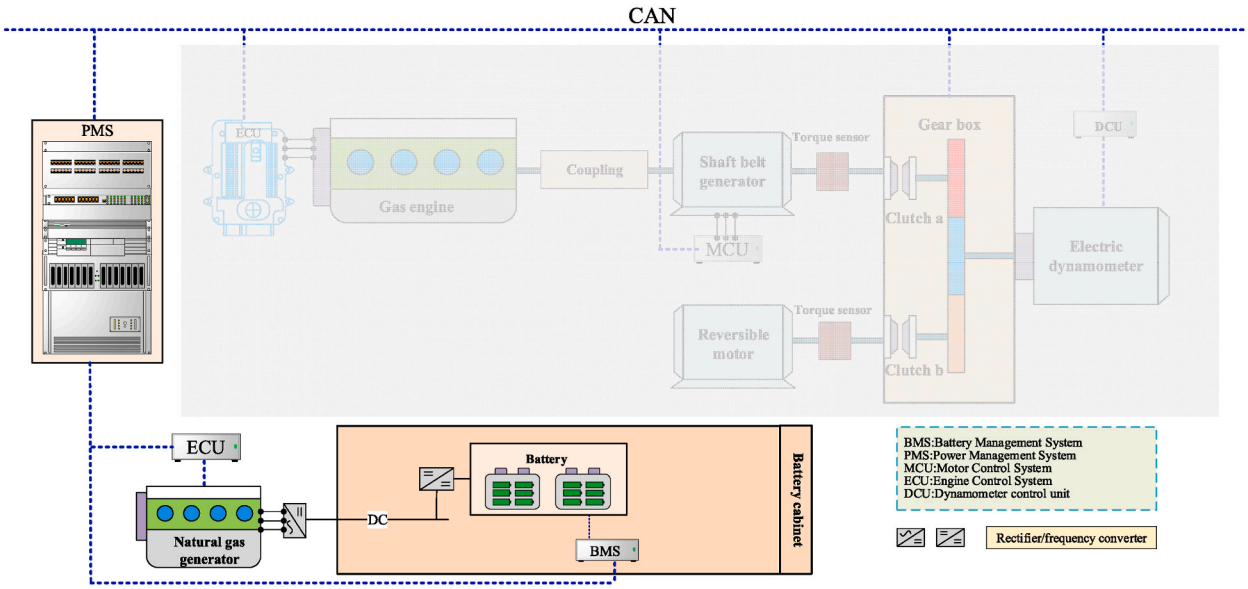

(a) work process

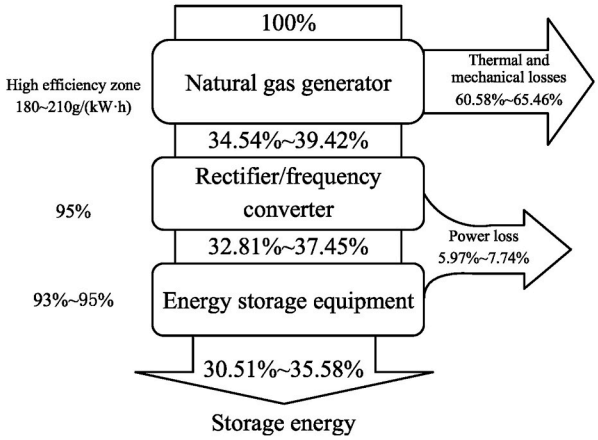

(b) Energy efficiency

Fig. 29. Natural gas generator charging mode.

propulsion mode significantly outperforming the gas-electric hybrid shaft generator-assisted propulsion mode. This underscores the importance of selecting the appropriate hybrid propulsion mode in hybrid power systems to achieve higher energy efficiency under varying operating conditions.

These conclusions serve as valuable guidance for enhancing the design and performance of hybrid gas-electric propulsion systems. They aid in the selection of the most suitable propulsion mode for specific applications, ultimately improving energy efficiency.

Hence, by aligning with specific application requirements, the design can be customized to match the rated power of the natural gas engine, ensuring adequacy for daily operational needs. In scenarios involving overload conditions, hybrid propulsion modes can be effectively harnessed to augment system performance, accommodating additional power demands and thereby optimizing energy efficiency across diverse operating conditions. This strategic approach is paramount for effective energy management and the performance optimization of hybrid gas-electric propulsion systems.

To visually compare the energy efficiency of the drive energy and stored energy across different operating modes, a bar chart is plotted, as shown in Fig. 30.

Table 3
Comparative analysis of energy efficiency in different modes.

Work mode	Sub-mode	Customized naming	Driving energy/ %	Storage energy/ %
Mechanical Propulsion Modes	Pure Mechanical Propulsion Mode	Mode 1	31.42–37.02	–
	Mechanical Propulsion with Reversible Electric Motor Generator Mode	Mode 2	31.42–37.02	25.51–31.37
	Mechanical Propulsion with Reversible Electric Motor Generator Mode II	Mode 3	31.42–37.02	28.01–33.47
	Mechanical Propulsion with Axial Belt Generator Mode	Mode 4	31.42–37.02	28.07–33.44
	Mechanical Propulsion with Axial Belt Generator Mode II	Mode 5	31.42–37.02	29.30–34.50
Electric Propulsion Modes	Gas Engine Electric Propulsion Mode	Mode 6	28.90–34.46	–
	Gas Engine Electric Propulsion Mode II	Mode 7	28.90–34.46	30.51–35.58
	Battery Electric Propulsion Mode	Mode 8	33.68–35.15	–
	Battery Electric Propulsion Mode II	Mode 9	26.40–31.44	–
	Gas-Electric Hybrid Electric Propulsion Mode	Mode 10	31.45–34.97	–
	Gas-Electric Hybrid Electric Propulsion Mode II	Mode 11	27.81–33.30	–
	Electric Propulsion with Axial Belt Generator Auxiliary Power Mode	Mode 12	28.90–34.43	28.05–33.41
	Electric Propulsion with Axial Belt Generator Auxiliary Power Mode II	Mode 13	28.90–34.43	29.28–34.49
	Gas Engine Generator Battery Electric Propulsion Mode	Mode 14	22.56–28.04	–
	Gas Engine Generator Battery Electric Propulsion Mode II	Mode 15	25.46–30.79	–
Hybrid Propulsion	Gas-Electric Hybrid Propulsion Mode	Mode 16	32.55–35.88	–
	Gas-Electric Hybrid Propulsion Mode II	Mode 17	28.90–34.03	–
	Gas-Electric Hybrid with Axial Belt Generator Auxiliary Power Propulsion Mode	Mode 18	26.99–32.53	–
	Gas-Electric Hybrid with Axial Belt Generator Auxiliary Power Propulsion Mode II	Mode 19	28.38–33.70	–
Charging Modes	Gas Engine Generator Charging Mode	Mode 20	–	28.05–33.41
	Gas Engine Generator Charging Mode II	Mode 21	–	29.43–34.85
	Natural Gas Generator Charging Mode	Mode 22	–	30.51–35.58

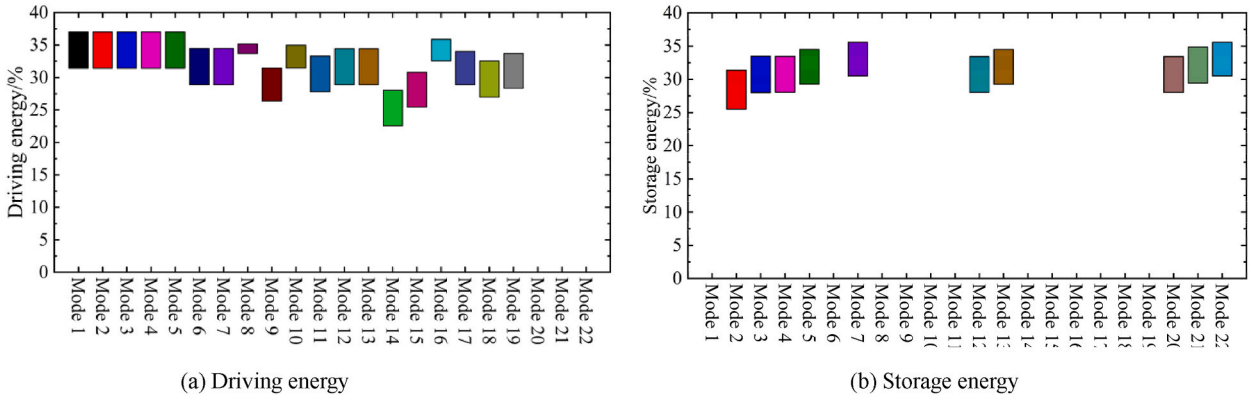

Fig. 30. Comparison of energy efficiency histograms in different modes.

5. Conclusion

This study investigates the energy efficiency of a series-parallel hybrid propulsion system for amphibious vehicles under different operating modes and power source conditions. The results are as follows.

(1) Operating modes involving natural gas engines demonstrate high performance, with energy efficiency reaching up to 37.02 %.
(2) Mechanical propulsion mode provides relatively efficient driving power across various conditions, with energy efficiency ranging from 31.42 % to 37.02 %.
(3) Electric propulsion mode achieves a maximum energy efficiency of 35.15 %, primarily due to the high operational efficiency of the electric motor.
(4) Hybrid propulsion mode effectively leverages the advantages of both power sources, with energy efficiency reaching up to 35.88 %.

Based on actual operational needs, the series-parallel hybrid system can be designed according to the rated power of the natural gas engine to meet daily operational requirements. For scenarios requiring additional power under overload conditions, the hybrid

propulsion mode can provide the necessary power, maximizing energy efficiency across different conditions. These findings provide important insights and guidance for the performance optimization and sustainable development of series-parallel hybrid systems.

Data availability statement

The authors do not have permission to share data.
The authors do not have any conflicts of interests/competing interests.

CRediT authorship contribution statement

Xiaojun Sun: Writing – review & editing, Writing – original draft, Validation, Project administration, Methodology, Funding acquisition. **Fengmei Xin:** Writing – review & editing, Software, Investigation, Formal analysis. **Kun Gao:** Methodology, Investigation.

Declaration of competing interest

The authors declare that they have no known competing financial interests or personal relationships that could have appeared to influence the work reported in this paper.

Acknowledgments

The author received funding for this study under the Doctoral Initiation Fund for Liaoning University of Technology (XB2023027).

References

[1] D. Pan, X. Xu, B. Liu, H. Xu, X. Wang, A review on drag reduction technology: focusing on amphibious vehicles, Ocean. Eng. 280 (2023) 114618, https://doi.org/10.1016/j.oceaneng.2023.114618.
[2] B. Liu, X. Xu, D. Pan, Influence of resistance due to locomotion mechanism configurations of a new high-speed amphibious vehicle (HSAV-II), Ocean. Eng. 283 (2023) 115175, https://doi.org/10.1016/j.oceaneng.2023.115175.
[3] S.-J. Lee, T. Lee, J.-J. Lee, W. Nam, J.C. Suh, Hydrodynamic characteristics of a hydrofoil-assisted amphibious vehicle, J. Ship Res. 61 (2017) 15–22. https://api.semanticscholar.org/CorpusID:125991087.
[4] L.F. Chuah, K. Mokhtar, S.M. Mhd Ruslan, A.A. Bakar, M.A. Abdullah, N.H. Osman, A. Bokhari, M. Mubashir, P.L. Show, Implementation of the energy efficiency existing ship index and carbon intensity indicator on domestic ship for marine environmental protection, Environ. Res. 222 (2023) 115348, https://doi.org/10.1016/j.envres.2023.115348.
[5] R. Derollepot, E. Vinot, Sizing of a combined series-parallel hybrid architecture for river ship application using genetic algorithm and optimal energy management, Math. Comput. Simulat. 158 (2019) 248–263, https://doi.org/10.1016/j.matcom.2018.09.012.
[6] G. Tang, J. Lei, F. Li, W. Zhu, X. Xu, B. Yao, C. Claramunt, X. Hu, A modified 6-DOF hybrid serial–parallel platform for ship wave compensation, Ocean. Eng. 280 (2023) 114336, https://doi.org/10.1016/j.oceaneng.2023.114336.
[7] X. Lü, S. He, Y. Xu, X. Zhai, S. Qian, T. Wu, Y. WangPei, Overview of improved dynamic programming algorithm for optimizing energy distribution of hybrid electric vehicles, Elec. Power Syst. Res. 232 (2024) 110372, https://doi.org/10.1016/j.epsr.2024.110372.
[8] X. Hu, L. Johannesson, N. Murgovski, B. Egardt, Longevity-conscious dimensioning and power management of the hybrid energy storage system in a fuel cell hybrid electric bus, Appl. Energy 137 (2015) 913–924, https://doi.org/10.1016/j.apenergy.2014.05.013.
[9] X. Sun, C. Yao, E. Song, Q. Yang, X. Yang, Optimal control of transient processes in marine hybrid propulsion systems: modeling, optimization and performance enhancement, Appl. Energy 321 (2022) 119404, https://doi.org/10.1016/j.apenergy.2022.119404.
[10] C. Xiao, B. Wang, C. Wang, Y. Yan, Design of a novel fully-active PEMFC-Lithium battery hybrid power system based on two automatic ON/OFF switches for unmanned aerial vehicle applications, Energy Convers. Manag. 292 (2023) 117417, https://doi.org/10.1016/j.enconman.2023.117417.
[11] C. Beatrice, C. Capasso, S. Doulgeris, Z. Samaras, O. Veneri, Hybrid storage system management for hybrid electric vehicles under real operating conditions, Appl. Energy 354 (2024) 122170, https://doi.org/10.1016/j.apenergy.2023.122170.
[12] M.F. Dogdu, I.A. Reyhancan, The comparison of gasoline powered vehicle and serial hybrid vehicle on emissions, Heliyon 10 (2024) e28532, https://doi.org/10.1016/j.heliyon.2024.e28532.
[13] H. Zhou, Z. Yu, X. Wu, Z. Fan, X. Yin, L. Zhou, Dynamic programming improved online fuzzy power distribution in a demonstration fuel cell hybrid bus, Energy 284 (2023) 128549, https://doi.org/10.1016/j.energy.2023.128549.
[14] Z. Liu, J. Zhao, Y. Qin, G. Wang, Q. Shi, J. Wu, H. Yang, Real time power management strategy for fuel cell hybrid electric bus based on Lyapunov stability theorem, Int. J. Hydrogen Energy 47 (2022) 36216–36231, https://doi.org/10.1016/j.ijhydene.2022.08.176.
[15] X. Sun, C. Yao, E. Song, Z. Liu, Y. Ke, S. Ding, Novel enhancement of energy distribution for marine hybrid propulsion systems by an advanced variable weight decision model predictive control, Energy 274 (2023) 127269, https://doi.org/10.1016/j.energy.2023.127269.
[16] C. Li, Z. Wang, H. Liu, F. Guo, C. Li, X. Xiu, C. Wang, J. Qin, L. Wei, Energy and configuration management strategy for solid oxide fuel cell/engine/battery hybrid power system with methanol on marine: a case study, Energy Convers. Manag. 307 (2024) 118355, https://doi.org/10.1016/j.enconman.2024.118355.
[17] C. Xiao, B. Wang, D. Zhao, C. Wang, Comprehensive investigation on Lithium batteries for electric and hybrid-electric unmanned aerial vehicle applications, Therm. Sci. Eng. Prog. 38 (2023) 101677, https://doi.org/10.1016/j.tsep.2023.101677.
[18] C. Yang, B. Liang, W. Wang, H. Wang, L. Yang, Y. Chen, M. Wang, An efficient energy management strategy based on heuristic dynamic programming specialized for hybrid electric unmanned delivery aerial vehicles, J. Clean. Prod. 453 (2024) 142222, https://doi.org/10.1016/j.jclepro.2024.142222.
[19] B. Liu, X. Xu, D. Pan, Resistance reduction optimization of an amphibious transport vehicle, Ocean. Eng. 280 (2023) 114854, https://doi.org/10.1016/j.oceaneng.2023.114854.
[20] B. Liu, D. Pan, X. Xu, Research on the resistance and maneuvering characteristics of an amphibious transport vehicle and the influence of stern hydrofoil, Ocean. Eng. 293 (2024) 116592, https://doi.org/10.1016/j.oceaneng.2023.116592.
[21] B. Liu, X. Xu, D. Pan, X. Wang, Research on shipping energy-saving technology: hydrofoil amphibious vehicle driven by waterjet propulsion, J. Clean. Prod. 382 (2023) 135257, https://doi.org/10.1016/j.jclepro.2022.135257.
[22] A. Kaleli, Development of the predictive based control of an autonomous engine cooling system for variable engine operating conditions in SI engines: design, modeling and real-time application, Control Eng. Pract. 100 (2020) 104424, https://doi.org/10.1016/j.conengprac.2020.104424.
[23] K. Wang, D. Zhang, Z. Shen, W. Zhu, H. Ye, D. Li, Novel ship fuel consumption modelling approaches for speed and trim optimisation: using engine data as auxiliary, Ocean. Eng. 286 (2023) 115520, https://doi.org/10.1016/j.oceaneng.2023.115520.

[24] S. Hänggi, T. Hilfiker, P. Soltic, R. Hutter, C. Onder, Control-oriented analysis of a lean-burn light-duty natural gas research engine with scavenged pre-chamber ignition, Combust. Engines. 1 (2019) 42–53, https://doi.org/10.19206/CE-2019-106.
[25] S.H. Rayasam, W. Qiu, T. Rimstidt, G.M. Shaver, D. Van Alstine, M. Graziano, Control-oriented modeling, validation, and interaction analysis of turbocharged lean-burn natural gas variable speed engine, Int. J. Engine Res. 24 (2021) 738–754. https://api.semanticscholar.org/CorpusID:245233042.
[26] C. Ma, C. Yao, E. Song, S.-L. Ding, Prediction and optimization of dual-fuel marine engine emissions and performance using combined ANN with PSO algorithms, Int. J. Engine Res. 23 (2021) 560–576. https://api.semanticscholar.org/CorpusID:234033344.
[27] Y. Lu, X. Han, Z. Chu, X. Feng, Y. Qin, M. Ouyang, L. Lu, A decomposed electrode model for real-time anode potential observation of lithium-ion batteries, J. Power Sources 513 (2021) 230529, https://doi.org/10.1016/j.jpowsour.2021.230529.
[28] H. He, R. Xiong, H. Guo, S. Li, Comparison study on the battery models used for the energy management of batteries in electric vehicles, Energy Convers. Manag. 64 (2012) 113–121, https://doi.org/10.1016/j.enconman.2012.04.014.